ENERGY-TURNS ANALYSIS

FOR A SCRAMJET POWERED MISSILE

by

Megaera C. Halter

Thesis submitted to the Faculty of the

Virginia Polytechnic Institute and State University

in partial fulfillment of the requirements for the degree of

MASTER OF SCIENCE

in

Aerospace Engineering

APPROVED:

E. M. Cliff, Chairman

F. H. Lutze

J. F. Marchman, III

May 1988

Blacksburg, Virginia

ENERGY-TURNS ANALYSIS

FOR A SCRAMJET POWERED MISSILE

by

Megaera C. Halter

E. M. Cliff, Chairman

Aerospace Engineering

(Abstract)

A reduced order model describing the energy and heading angle dynamics of a scramjet missile is developed using a singular perturbation technique. The cruise analysis is briefly reviewed to determine the conditions at which the missile will cruise most efficiently. The turn and climb performance of the missile over the conditions of interest is then examined and a family of extremal trajectories is constructed which asymptotically approach the cruise at an intermediate altitude.

ACKNOWLEDGEMENTS

I would like to thank Dr. Cliff for his patience during many long-distance discussions. Thanks also to Drs. Lutze, Kelley and Marchman for being on my committee.

To Hugh and Janet -- all that moral support really did help. And those late night technical debates with Ron cleared my thoughts and boosted my morale.

CONTENTS

LIST OF TABLES

LIST OF FIGURES

LIST OF SYMBOLS

a	- speed of sound
a	- coefficient multiplying the energy characteristic vector of the linearized system
A_O/A_I	- engine capture ratio
b	- coefficient multiplying the heading characteristic vector of the linearized system
C_D	- drag coefficient
C_{D_0}, C_{D_2}	- coefficients of drag-polar
C_L	- lift coefficient
C_{L_D}	- interior candidate for minimizing lift
C_T	- engine-off thrust coefficient
C_{xe}	- inlet drag coefficient
e	- engine propulsive efficiency
E	- specific energy
F_A	- fuel-to-air ratio for stoichiometric combustion
h	- altitude
H	- Hamiltonian, pseudo-Hamiltonian
I_{sp}	- specific impulse
J	- performance index
L	- lift
L	- lapse rate for atmospheric temperature
M	- Mach number
n	- load factor

q	- dynamic pressure
Q_{STO}	- stoichiometric fuel flow rate
R	- range; $R = \sqrt{x^2 + y^2}$
R	- gas constant for air
S	- characteristic area for aerodynamics
S_e	- engine inlet area
S_i	- generic state-variable
t	- time
$\mathcal{T}$	- stretched time for the inner boundary layer
T	- thrust
T_0	- sea level atmospheric temperature
u	- general control
$\underline{u}_i$	- characteristic vector of the linearized E-χ system
V	- velocity; $[2g(E-h)]^{1/2}$
w_i	- coefficients of the specific impulse polynomial
W	- missile weight
W_F	- weight of fuel consumed
x	- downrange distance
$\underline{x}_e$	- equilibrium value of the state-costate vector
y	- crossrange distance

Greek and Other Symbols

β_i - inequality constraint

γ - flight path angle

γ - ratio of specific heats for air

δ - perturbation from equilibrium

ε_i - perturbation parameters for order reduction

η - throttle

λ_i - adjoint states, constraint multipliers

μ - bank angle

ρ - atmospheric density

σ_i - characteristic value of the linearized E-χ system

τ - stretched time for energy-turn boundary layer

χ - heading angle

$\partial(\ )/\partial(\ )$ - partial derivative

Subscripts

$(\ )_{EFF}$ - fuel-efficient

$(\ )_f$ - quantity at final time

$(\ )_{max}$ - maximum value

$(\ )_0$ - quantity at initial time

$(\ )_{sust}$ - sustainable

Superscripts

$(\bar{\ })$ - quantity from solution to outer problem, constraining value

$(\tilde{\ })$ - quantity from solution to energy-turn problem

$(\dot{\ })$ - time derivative

CHAPTER 1. INTRODUCTION

Increasingly, aircraft and missiles must complete missions which are so demanding that the proper strategy for flying the mission must be designed as carefully as the hardware. An ideal example of this is the National Aerospace Plane, which will be required to fly repeatedly from the ground to orbit and back with moderate fuel expenditure. To successfully carry out these missions, a thorough understanding of the proper trajectories and control strategies will be needed as the design progresses.

In past years, substantial improvements in performance could be achieved by improving components of the vehicle; design a more efficient wing, a more powerful engine, a lighter structure. The issue of flight strategy was addressed after the hardware design was complete, and for most missions, required relatively simple analysis. But as the vehicles become more complex and the missions more demanding, designers must consider strategies to extract the most performance out of the designs. This can be addressed in two stages. First, the trajectories which exploit the kinematic capabilities of the vehicle must be determined. Secondly, control and guidance laws must be formulated so that the vehicle will fly as close as practical to those capabilities. The first consideration is dealt with in this thesis, in the context of a long range, high speed missile.

Tactical missiles are being required to engage higher speed targets at greater distances, while subject to severe limitations on initial size and weight. For a typical mission, these conflicting requirements

can be expressed as: be able to engage targets as far away as possible, to get there quickly, and to do this with a limited amount of fuel. Many avenues are being pursued to accomplish this, among them the use of ramjet engines rather than solid rockets. Ramjets have the twin advantages of using atmospheric oxygen as oxidizer, thus reducing launch weight, and having throttleable thrust, which allows much finer scheduling of speeds for efficient flight. Because of the complex physics and conflicting requirements, this type of problem is suitable for optimization. The consequences of changing emphasis on different requirements can be seen, frequently yielding unexpected results.

A consequence of the long range trajectories, and hence, the long flight times, is the need to be able to change heading or cruise condition midway through the flight in a manner consistent with the overall flight objectives. This situation could arise several ways, among them being the need to steer out heading errors which have accumulated since launch. Another possibility is that the target may have maneuvered substantially and the missile would have to compensate during cruise. A third possibility is that the missile may be retargeted to another target in the vicinity of the original. For situations of this type, where the cruise is being adjusted, it is interesting to look at the turning and climbing capabilities of the missile.

In this thesis, the energy and heading angle rates are examined for a long range, high speed missile with a ramjet engine. This is a continuation of past studies which deal with the performance of this missile in the vertical plane. In [7], Cliff, Kelley and Lutze examine

the overall optimal trajectories for the missile in the vertical plane. Chichka considers the cruise-dash performance in [5]. Reference [13], by Shankar, is a study of the altitude-flight path angle dynamics. Other related work include [8] by Hedrick and Bryson in which the minimum energy-heading angle trajectories of a supersonic aircraft are examined. Cliff, Kelley and Lefton [6] consider the minimum time energy-turn performance of an aircraft equipped with thrust vectoring.

In this paper, the choice of optimization problem is briefly reviewed. The equations of motion for the vehicle and several constraints dictated by the capabilities of the missile are introduced. The point mass model is then reduced in order by means of singular perturbations to three simpler problems: cruise-dash, energy-heading angle and altitude-flight path angle. The subproblem of interest is the second, which describes the dynamics of changing heading angle and specific energy. In the third chapter, the adjoint differential equations and minimizing controls for extremal trajectories are developed using the minimum principle.

The maximum point performance for the missile according to this reduced order model is examined in the fourth chapter. Fastest climb, most economical climb and fastest turn are discussed. In the fifth chapter, a family of extremal trajectories which fair smoothly into a selected cruise are presented.

Finally, the results are summarized and suggestions are made for future work.

CHAPTER 2. FORMULATION

Choice of Optimization Problem

For long range flight there are two conflicting requirements. Assuming the fuel on board is fixed, targets are to be engaged as far away as possible (maximize range), and as quickly as possible (minimize time elapsed). A balance among these requirements can be expressed as the following Mayer problem: minimize the weighted sum of time elapsed and fuel consumed to fly a specified distance.

$$J = \mu_t t_f + \mu_f W_F(t_f) \qquad \mu_t,\ \mu_F \geq 0 \qquad (1)$$

subject to the final-time constraints:

$$\begin{aligned} x(t_f) - x_f &= 0 \\ y(t_f) - y_f &= 0 \\ h(t_f) - h_f &= 0 \end{aligned} \qquad (2)$$

The original problem statement has been replaced by the closely related problem [7] of minimizing the sum of fuel consumed and time elapsed while flying to a specified point. The weighting factors, μ_t and μ_F, allow choice of the relative importance of the two quantities. Increasing μ_t places more emphasis on short flight time and will result in a trajectory with faster average velocity at the expense of extra fuel. Conversely, a bigger μ_F will reduce the fuel consumption while

probably increasing the flight time. For a given final position, the proper choice of weights would be those which lead to intercept just as fuel is exhausted (with perhaps a little left over for terminal maneuvers). The choice of proper multipliers for a particular engagement is a fire control problem and is not addressed in this paper.

Point Mass Model and Constraints

The equations of motion for the missile are:

$$\dot{h} = V \sin\gamma \tag{3}$$

$$\dot{\gamma} = \frac{g}{V}\left[\frac{(L + T \sin\alpha)\cos\mu}{W_o - W_F} - \cos\gamma\right] \tag{4}$$

$$\dot{E} = \frac{V\left(T - D + T(\cos\alpha - 1)\right)}{W_o - W_F} \tag{5}$$

$$\dot{\chi} = \frac{g}{V\cos\gamma}\left[\frac{L \sin\mu + T \sin\alpha \sin\mu}{W_o - W_F}\right] \tag{6}$$

$$\dot{x} = V \cos\gamma \cos\chi \tag{7}$$

$$\dot{y} = V \cos\gamma \sin\chi \tag{8}$$

$$\dot{W}_F = \eta\, Q_{STO} \tag{9}$$

The states are altitude, h; flight path angle, γ; specific energy, E; heading angle, χ; range, x; crossrange, y; and fuel consumed, W_F. The controls are lift coefficient, C_L; throttle, η; and bank angle, μ. The specific energy, or energy height, is the sum of kinetic and

potential energies, normalized by weight.

$$E = \frac{V^2}{2g} + h$$

Since Kaiser introduced energy-height for performance analysis of aircraft climb [10], this has been a popular variable in analyses of this type [7, 8, 11]. For conciseness in the rest of this paper, this quantity will be referred to as "energy".

The following assumptions are implicit in these equations:

- body dynamics neglected
- flat Earth
- no winds
- coordinated maneuvers, i.e. zero side force
- thrust along missile axis of symmetry

In addition to the differential equations above, several inequality constraints reflecting physical limitations must also be considered.

β_1:	$h - h_T \geq 0$	terrain limit	(10)
β_2:	$h - \bar{h}(M) \geq 0$	Mach - dynamic pressure limit	(11)
β_3:	$\bar{C}_L - C_L \geq 0$	aerodynamic limit	(12)
β_4:	$\bar{n}\, W - L \geq 0$	structural limit	(13)
β_5:	$\dot{\bar{W}}_F - \eta Q_{STO} \geq 0$	fuel flow limit	(14)

The fifth limit, β_5, is an upper limit on the mass flow rate of the

fuel into the engine, $\dot{\bar{W}}_F$, a specified constant. Additionally, the throttle must be either off, $\eta = 0$, or within the operating range, $\eta_{min} \leq \eta \leq \eta_{max}$. Details of the aerodynamic and propulsive models are discussed in the Appendix.

Figures (2-1) and (2-2) illustrate these constraints for h vs. E and, more typically, for h vs. V. The terrain limit, h_T, is a constant which prevents the missile from flying at altitudes below ground level. The second low altitude limit, $\bar{h}$, is a function of Mach number which places an upper limit on the combination of Mach number and dynamic pressure which can be reached. This limit was provided with the other missile data. Also illustrated are upper limits on dynamic pressure ($\bar{q}$ = 18,000 lb/ft^2) and Mach number ($\bar{M}$ = 6). For low values of $\bar{M}$, the slope of the constraint is always positive and the function is always a lower bound on altitude. However, for large M the behavior is qualitatively different. For altitudes within the troposphere, the energy at which the Mach number constraint is active *decreases* with altitude. At higher altitudes, the slope of the constraint is positive. The result is that this constraint will be satisfied at two altitudes for a given energy. The value of $\bar{M}$ at which the character of the constraint changes can be determined by differentiating it with respect to altitude and equating to zero.

$$E = h + a^2(h)\frac{\bar{M}^2}{2g} = h + \frac{\bar{M}^2\gamma R}{2g}(T_0+Lh)$$

where, T_0 = sea level air temperature

L = temperature lapse rate

γ = ratio of specific heats for air

R = gas constant for air

$$\frac{dE}{dh} = 1 + \frac{\bar{M}^2\gamma RL}{2g} = 0$$

$$\bar{M}^2 = \frac{2g}{\gamma RL} \approx 2.76$$

A consequence of the double-valued property of the Mach number constraint for $\bar{M} = 6$ is that the constraint is not always a lower bound on altitude. To avoid difficulties which this would introduce later in the analysis, the more restrictive Mach-dynamic pressure limit, $\bar{h}$, will be used.

The third and fourth constraints are upper limits on the magnitude of the lift coefficient. The aerodynamic limit, $\bar{C}_L$, is a specified function of Mach number and is discussed in the Appendix. The structural limit prevents the missile from flying in conditions which would cause structural failure, and is imposed by limiting the load-factor to be less than a specified constant, $\bar{n}$. Also plotted in Figures (2-1) and (2-2) is the corner velocity locus [11], where the missile is banked such that both the structural and aerodynamic limits are active. This is an ideal condition for rapid turns. Because of the restrictive $\bar{h}$ limit, the corner-velocity locus can be reached for only a small band of energies. For altitudes below corner-velocity

locus, the structural limit is the more restrictive constraint on lift coefficient. Above this locus, the atmospheric density is lower and the lift coefficient is bounded by the aerodynamic limit.

The loft-ceiling is the highest altitude at which lift can sustain weight in level flight. Note that the curve representing the highest altitude at which thrust equals drag does not appear on either of these figures. This missile has ample thrust.

The minimization problem, subject to the above differential equations and constraints, is difficult to solve in its present form. First, the total system of differential equations, including adjoint states to be introduced shortly, is fifteenth order, and is subject to several constraints. Second, the system is "stiff". Some states, such as position vary much more slowly than others, such as flight path angle. To numerically integrate a system such as this, a small time step is needed to capture the high frequency dynamics and a large computational word length is needed to prevent the slow dynamics from becoming unstable.

When the rates at which the states vary cluster into two or more widely separated groups, the problem can be split into several reduced order sub-problems by means of *singular perturbations* [1, 4, 11, 14]. These simpler problems come with a price. In each sub-problem the dynamics and boundary values of the fast motions are lost, possibly leading to instantaneous jumps in some of those variables. However, the different solutions can frequently be faired together to form a composite solution which will approximate the solution to the full order problem quite closely. In the next section, the full problem will

be set up to be split into three sub-problems.

The Full Problem

Kelley was one of the first researchers to apply singular perturbation theory to problems in flight mechanics.[11] The following development closely resembles that in [11].

For this method to be effective, the state variables must cluster into groups of similar rates and these rates must be well separated from each other. This motivates the choice of specific energy as a state instead of velocity.

$$E = \frac{V^2}{2g} + h \qquad (15)$$

The slowest states, x, y, and W_F, form the outer, or cruise-dash problem. The boundary layer, or energy-heading angle problem, deals with the changing total energy of the system and with the dynamics of the heading angle, χ. The two fastest states, h and γ, form the inner boundary layer. The problem of interest here is the E-χ boundary layer. To get to that, the overall optimization problem is set up.

To do this, small parameters which correspond to the grouping above must be in the equations of state. Since they do not occur naturally, the small parameters ε_1 and ε_2 will be artificially inserted.

$$\varepsilon_2 \dot{h} = V \sin\gamma \tag{16}$$

$$\varepsilon_2 \dot{\gamma} = \frac{g}{V} \left[\frac{(L + \varepsilon_3 T \sin\alpha) \cos\mu}{W_o - \varepsilon_3 W_F} - \cos\gamma \right] \tag{17}$$

$$\varepsilon_1 \dot{E} = \frac{V \left(T - D + \varepsilon_3 T (\cos\alpha - 1)\right)}{W_o - \varepsilon_3 W_F} \tag{18}$$

$$\varepsilon_1 \dot{\chi} = \frac{g \sin\mu}{V \cos\gamma} \left[\frac{L + \varepsilon_3 T \sin\alpha}{W_o - \varepsilon_3 W_F} \right] \tag{19}$$

$$\dot{x} = V \cos\gamma \cos\chi \tag{20}$$

$$\dot{y} = V \cos\gamma \sin\chi \tag{21}$$

$$\dot{W}_F = \eta \, Q_{STO} \tag{22}$$

where, $\varepsilon_2 << \varepsilon_1 << 1$

$$V = \sqrt{2g\,(E - h)}$$

Note that in the equations above, a third small parameter, ε_3, has been introduced. With this, the effects of thrust angle with respect to the flight path and of variable mass can be treated as ordinary perturbations. Throughout the rest of this paper ε_3=0. This simplifies the analysis but does not result in order reduction.

The extremizing controls will be found by applying the minimum principle [3, pg.108 and 12, pg. 25]. Form the pseudo-Hamiltonian for this system

$$
\left.
\begin{aligned}
&H = H^0 + H^1 + H^2 + \Sigma\, \lambda_i \beta_i \quad , \quad i = 1,5 \\
&\quad \text{where,} \\
&\qquad H^0 = (-\lambda_x \cos\chi + \lambda_y \sin\chi) V \cos\gamma + \lambda_F \eta\, Q_{STO} \\
&\qquad H^1 = \lambda_E \frac{V(T - D)}{W_0} + \lambda_\chi \frac{g\, L \sin\mu}{W_0 V \cos\gamma} \\
&\qquad H^2 = \lambda_h V \sin\gamma + \lambda_\gamma \frac{g}{V} \left[\frac{L\cos\mu}{W_0} - \cos\gamma \right]
\end{aligned}
\right\} \quad (23)
$$

The Euler-Lagrange conditions provide necessary conditions for an extremum [3 pg. 49]. First, the adjoint multipliers above must satisfy the following differential equations.

$$
\left.
\begin{aligned}
&\epsilon_2 \dot{\lambda}_h = -\frac{\partial H}{\partial h} \qquad \epsilon_2 \dot{\lambda}_\gamma = -\frac{\partial H}{\partial \gamma} \\
&\epsilon_1 \dot{\lambda}_E = -\frac{\partial H}{\partial E} \qquad \epsilon_1 \dot{\lambda}_\chi = -\frac{\partial H}{\partial \chi} \\
&-\dot{\lambda}_x = -\frac{\partial H}{\partial x} \qquad \dot{\lambda}_y = -\frac{\partial H}{\partial y} \qquad \dot{\lambda}_F = -\frac{\partial H}{\partial W_F}
\end{aligned}
\right\} \quad (24)
$$

The extremizing controls must satisfy:

$$
\frac{\partial H}{\partial \eta} = 0 \qquad \frac{\partial H}{\partial \mu} = 0 \qquad \frac{\partial H}{\partial C_L} = 0 \qquad (25)
$$

Since the Hamiltonian is not an explicit function of time, there is a first integral: H is constant.

To solve this fifteenth order system of differential equations (including time), fifteen boundary conditions are needed. The initial values of the state and the final position provide ten conditions. The rest are provided by transversality. Recall from equation (1),

$$J = \mu_t t_f + \mu_f W_F(t_f)$$

$$\left\{ \frac{\partial J}{\partial t} + H \right\}_{t_f} = 0 \quad \text{yields} \quad H = -\mu_t \tag{26}$$

$$\left\{ \frac{\partial J}{\partial x_i} \right\}_{t_f} = \lambda_i \quad \text{yields} \quad \left.\begin{aligned} &\lambda_F(t_f) = \mu_F \\ &\lambda_E(t_f) = \lambda_\chi(t_f) = 0 \\ &\lambda_\gamma(t_f) = 0 \end{aligned}\right\} \tag{27}$$

Note that the boundary conditions are split between initial and final time. The two point boundary value problem is now ready for order reduction.

Outer Problem: Cruise-Dash

To reduce the full problem to cruise-dash, which deals with the time histories of position and fuel consumption, allow ε_1 and ε_2 in equations (16) through (24) to approach zero. The result is that six differential equations remain, those for x, y, W_F and the associated adjoint states. The differential equations for the "faster" states have become algebraic equality constraints, the associated states are demoted to controls, and the Euler-Lagrange equations for the adjoints now serve to determine what values these pseudo-controls must have to be extremizing. After some manipulation,

$$\dot{x} = V \cos\gamma \cos\chi$$

$$\dot{y} = V \cos\gamma \sin\chi$$

$$\dot{W}_F = \eta \, Q_{STO}$$

$$\lambda_y = - \lambda_x \tan\chi = \text{constant}$$

$$\tan\chi = \frac{y_f - y_o}{x_f - x_o}$$

$$\lambda_F = \mu_F = \text{constant}$$

The solution to this problem is discussed further in Chapter 4 and in detail in [5].

Boundary Layer: Energy-Heading Angle

The boundary layer equations result when a time stretching transformation, $\tau = t/\varepsilon_1$, is introduced and both ε_1 and $\varepsilon_2/\varepsilon_1$ are then allowed to approach zero. Note that since ε_2 is specified to be "much smaller" than ε_1, it will approach zero more rapidly. The resulting equations are:

$$V \sin\gamma = 0 \qquad (28)$$

$$\frac{L\cos\mu}{W_o} - \cos\gamma = 0 \qquad (29)$$

$$\dot{E} = \frac{V(T - D)}{W_o} \qquad (30)$$

$$\dot{\chi} = \frac{g\ L\ \sin\mu}{W_o V\ \cos\gamma} \qquad (31)$$

$$\dot{x} = \dot{y} = \dot{W}_F = 0 \qquad (32)$$

Altitude and flight path angle are control-like in this boundary layer and the equality constraints (28) and (29) resulting from their differential equations will simplify the E and χ equations. The cruise states are now constants, the values of which are determined by the cruise-dash solution. In this boundary layer, these values will be denoted by $(\bar{\ })$. Since x, y and W_F are all ignorable, reducing them to constants does not simplify the differential equations for E and χ. The pseudo-Hamiltonian has three terms:

$$H = H^1 + H^0 + \Sigma\ \lambda_i\beta_i \quad , \quad i = 1,5$$

$$H = \lambda_E \frac{V(T - D)}{W_o} + \lambda_\chi \frac{g\ L\ \sin\mu}{W_o V\ \cos\gamma} \qquad (33)$$

$$+\{(-\bar{\lambda}_x\cos\chi + \bar{\lambda}_y\sin\chi)V\cos\gamma + \bar{\lambda}_F\eta\ Q_{STO}\}$$

$$+ \Sigma\ \lambda_i\beta_i \quad , \quad i = 1,5$$

The term set off in braces is inherited from the cruise-dash portion,

and serves to link this boundary layer to the outer problem in which it is nested. Effectively, an integral term has been added to the cost to be minimized in this subproblem [11]:

$$J = \mu_t t_f + \mu_F W_F(t_f) \qquad (34)$$

$$+ \int_{\tau_0}^{\tau\to\infty} \{(-\bar{\lambda}_x \cos\chi + \bar{\lambda}_y \sin\chi) V\cos\gamma + \bar{\lambda}_F \eta\, Q_{STO}\}\, dt$$

The initial conditions for E and χ are those of the original, unreduced problem and the values of these variables for $\tau\to\infty$ are the initial values from the cruise solution.

This boundary layer is the main topic of this paper and will be addressed in more detail in the next chapter. Note that the simpler problem of energy transitions without turning was addressed for this missile in [6]. For completeness, the formulation of the inner boundary layer will be briefly reviewed.

Inner Boundary Layer: Altitude-Flight Path Angle

To form this inner boundary layer, a second time stretching variable is introduced, $\mathcal{T} = t/\varepsilon_2$. Repeating the procedure above, the differential equations for h, γ, λ_h, and λ_γ remain. The states associated with the two slower problems are treated as constants whose values are determined by the solutions of the corresponding subproblems. The Hamiltonian has all the terms indicated in equations

(23), where the terms pertaining to the cruise-dash and energy-heading angle subproblems are integral terms added to the cost.

$$J = \mu_t t_f + \mu_F W_F(t_f) \tag{35}$$

$$+ \int_{\mathcal{T}_0}^{\mathcal{T}\to\infty} \{(-\bar{\lambda}_x \cos\chi + \bar{\lambda}_y \sin\chi) V \cos\gamma + \bar{\lambda}_F \eta \, Q_{STO}\} \, dt$$

$$+ \int_{\mathcal{T}_0}^{\mathcal{T}\to\infty} \left\{ \tilde{\lambda}_E \frac{V(T - D)}{W_0} + \tilde{\lambda}_\chi \frac{g \, L \sin\mu}{W_0 V \cos\gamma} \right\} dt$$

In this chapter the full optimization problem and the three reduced-order problems have been introduced. These problems were previously addressed in the vertical plane for this missile, but with a different aerodynamic formulation. In [5], the cruise-dash problem is discussed in detail, the energy boundary layer without turning is analyzed in [7], and in [13], the altitude-flight path boundary layer is analyzed. In the next chapter, the details of solving the energy-heading angle boundary layer are set up.

CHAPTER 3. SOLUTION PROCEDURE FOR THE ENERGY - TURNS LAYER

State-Adjoint System

The reduced order problem was set up in equations (28) through (34). From equations (28) and (29), the following equality constraints result.

$$\gamma = 0 \tag{36}$$

$$L = W_0 \sec\mu \tag{37}$$

The first will be applied by direct substitution throughout the problem. The second will be appended to the pseudo-Hamiltonian using the Valentine method [9, pg. 262]. After a little algebra, the system of equations becomes,

$$\dot{E} = \frac{V(T - D)}{W_0} \tag{38}$$

$$\dot{\chi} = \frac{g \tan\mu}{V} \tag{39}$$

$$H_0 = \lambda_E \frac{V(T - D)}{W_0} + \lambda_\chi \frac{g \tan\mu}{V} \tag{40}$$

$$+\{(-\bar{\lambda}_x \cos\chi + \bar{\lambda}_y \sin\chi)V + \bar{\lambda}_F \eta\, Q_{STO}\}$$

$$H = H_0 + \lambda_1(h - h_T) + \lambda_2(h - \bar{h}) + \lambda_3(\bar{C}_L - C_L) \tag{41}$$

$$+ \lambda_4(\bar{n}\, W_0 - L) + \lambda_5(\dot{\bar{W}}_F - \eta\, Q_{STO}) + \lambda_L(L - W_0 \sec\mu)$$

Applying equations (24) and (25) to the pseudo-Hamiltonian yields the adjoint and the control equations.

$$\dot{\lambda}_\chi = -(\bar{\lambda}_x \sin\chi + \bar{\lambda}_y \cos\chi)V \tag{42}$$

$$\dot{\lambda}_E = -\frac{\lambda_E}{W_0}\left[\frac{\partial V}{\partial E}(T - D) + V\left(\frac{\partial T}{\partial E} - \frac{\partial D}{\partial E}\right)\right] + \frac{\lambda_\chi\, g \tan\mu}{V^2}\frac{\partial V}{\partial E} \tag{43}$$

$$+ (\bar{\lambda}_x \cos\chi - \bar{\lambda}_y \sin\chi)\frac{\partial V}{\partial E} - (\bar{\lambda}_F - \lambda_5)\eta\, \frac{\partial Q_{STO}}{\partial E}$$

$$+ \lambda_2 \frac{\partial \bar{h}}{\partial E} - \lambda_3 \frac{\partial \bar{C}_L}{\partial E} + (\lambda_4 - \lambda_L)C_L S\, \frac{\partial q}{\partial E}$$

$$\frac{\partial H}{\partial \eta} = 0 = \frac{\lambda_E V}{W_0}\frac{\partial T}{\partial \eta} + (\bar{\lambda}_F - \lambda_5)Q_{STO} \tag{45}$$

$$\frac{\partial H}{\partial C_L} = 0 = -\frac{2\lambda_E V}{W_0} C_{D_2} C_L q S + (\lambda_L - \lambda_4) q\, S - \lambda_3 \tag{46}$$

$$\frac{\partial H}{\partial \mu} = 0 = \frac{\lambda_\chi\, g}{V} - \lambda_L W_0 \sin\mu \tag{47}$$

$$\frac{\partial H}{\partial h} = 0 = \frac{\lambda_E}{W_o}\left[\frac{\partial V}{\partial h}(T - D) + V\left(\frac{\partial T}{\partial h} - \frac{\partial D}{\partial h}\right)\right] - \frac{\lambda_\chi\, g \tan\mu}{V^2}\frac{\partial V}{\partial h} \qquad (48)$$

$$+ (-\bar{\lambda}_x \cos\chi + \bar{\lambda}_y \sin\chi)\frac{\partial V}{\partial h} + (\bar{\lambda}_F - \lambda_5)\eta\,\frac{\partial Q_{STO}}{\partial h}$$

$$+ \lambda_1 + \lambda_2\left(1 - \frac{\partial \bar{h}}{\partial h}\right) + \lambda_3\frac{\partial \bar{C}_L}{\partial h} - (\lambda_4 - \lambda_L)C_L S\,\frac{\partial q}{\partial h}$$

Altitude Determination

As the states, E and χ, and the adjoints, λ_E and λ_χ, are integrated forward in time, equations (45) through (47) can be solved explicitly for the extremizing controls. The altitude equation is complex, however, and must be solved numerically. For this reason, it is appropriate to separate the minimization procedure into three nested steps.

$$\min_{h, C_L, \mu, \eta} H = \min_{h}\left\{\min_{C_L, \mu}\left(\min_{\eta} H\right)\right\} \qquad (49)$$

The cruise multipliers $\bar{\lambda}_X$, $\bar{\lambda}_Y$, $\bar{\lambda}_F$ are specified by the outer problem and at each time step, E, χ, λ_E and λ_χ are fixed. A one-dimensional search is used to find the minimizing altitude, where at each altitude the pseudo- Hamiltonian is minimized with respect to the other controls. This minimum must b forund *precisely*. Figure (3-1) illustrates a typical profile of H vs. altitude, where at each altitude the operation in the braces of equation (49) has been performed. For the case illustrated, λ_χ has been set to weight turning rate rather heavily compared to energy rate, and E and χ are fixed. In general there are several possible candidates for minimizing altitude:

the low altitude constraint, the loft ceiling, the corner-velocity altitude and an interior minimum. For the particular combination of conditions in Figure (3-1), the the corner-velocity altitude is minimizing.

If one of the low altitude constraints is active, the associated multipliers are determined as follows: For terrain limit active,

$$\lambda_1 = -\left(\frac{\partial H_o}{\partial h} - \lambda_S \eta \frac{\partial Q_{STO}}{\partial h} + \lambda_L C_L S \frac{\partial q}{\partial h} \right) \qquad (50)$$

Similarly, if the Mach-altitude limit is active, the multiplier λ_2 follows from $\bar{h}$, which is a function of M.

$$\lambda_2 = \frac{-\left(\frac{\partial H_o}{\partial h} - \lambda_S \eta \frac{\partial Q_{STO}}{\partial h} + \lambda_L C_L S \frac{\partial q}{\partial h} \right)}{\left(1 - \frac{\partial \bar{h}}{\partial h} \right)} \qquad (51)$$

Note that all derivatives must be evaluated for fixed energy and heading angle. The peculiar derivative $(\partial\bar{h}/\partial h)$ is evaluated as the product $(\partial\bar{h}/\partial M)(\partial M/\partial h)$, where energy is fixed. See the Appendix.

Throttle Determination

Equation (45) is a quadratic in throttle.

$$3\, w_2 \eta^2 + 2\, w_1 \eta + \left(w_o + \frac{(\bar{\lambda}_F - \lambda_S) W_o}{\lambda_E V e} \right) = 0 \qquad (52)$$

There are up to five candidates for minimizing throttle: 0, η_{min}, the smaller of $\dot{W}_F/Q_{STO}$ and η_{max}, and those roots of equation (52) which are real and within the constraints. The choice of best throttle must be made by direct comparison of the pseudo-Hamiltonian at each throttle. If β_5 is active then equation (52) can be solved for the value of the constraint multiplier, λ_5.

Lift Coefficient and Bank Angle Determination

The procedure which follows is intricate. First, determine the bank angle by evaluating equation (37). If $\mu = 0$, the structural limit cannot be active (λ_4=0). If, in addition, the aerodynamic limit is inactive, then λ_3=0 and the Valentine multipier λ_L can be found from equation (46).

$$\lambda_L = \frac{2\lambda_E V}{W_o} C_{D_2} C_L$$

If μ=0 and the aerodynamic constraint is active, the altitude is equal to the loft ceiling and equations (46) and (48) combine to yield

$$\lambda_L = - \frac{\frac{1}{S}\left(\frac{\partial H_o}{\partial h} - \lambda_5 \eta \frac{\partial Q_{STO}}{\partial h} \right) - \frac{2\,\lambda_E C_{D_2} C_L q}{W_o} \frac{\partial \bar{C}_L}{\partial h}}{\left(q \frac{\partial \bar{C}_L}{\partial h} + C_L \frac{\partial q}{\partial h} \right)} \qquad (53)$$

If $\mu \neq 0$, λ_L results from equation (47),

$$\lambda_L = \frac{\lambda_\chi g}{W_o V \sin\mu} \qquad (54)$$

There are four possible minimizing lift conditions. First, an interior minimium, which, after some algebra, is:

$$C_{L_D} = \sqrt{\left(\frac{W_o}{q\,S}\right)^2 + \left(\frac{\lambda_\chi g}{2\lambda_E V^2 C_{D_2}}\right)^2} \qquad (55)$$

The other alternatives are aerodynamic limit active, structural limit active or both. If the aerodynamic limit alone is active, $C_L = \bar{C}_L(M)$, $\lambda_4 = 0$ and

$$\lambda_3 = \left(\lambda_L - \frac{2\lambda_E V C_{D_2} C_L}{W_o}\right) q\,S \qquad (56)$$

If the structural limit alone is the active constraint, $C_L = \frac{\bar{n}\,W}{q\,S}$, $\lambda_3 = 0$ and

$$\lambda_4 = \lambda_L - \frac{2\lambda_E V C_{D_2} C_L}{W_o} \qquad (57)$$

At the corner velocity, both aerodynamic and structural limits are active. This condition will occur only during banked flight, and, for fixed energy, at a unique altitude. Solving equations (46) and (48) for λ_3

and λ_4 results in

$$\lambda_3 = - \frac{\left(\frac{2\,\lambda_E V C_{D_2} C_L^2 S}{W_o} \frac{\partial q}{\partial h} + \frac{\partial H_o}{\partial h} - \lambda_5 \eta \frac{\partial Q_{STO}}{\partial h} \right)}{\left(\frac{\partial \bar{C}_L}{\partial h} + \frac{C_L}{q} \frac{\partial q}{\partial h} \right)} \qquad (58)$$

and

$$\lambda_4 = \lambda_L - \frac{2\lambda_E V C_{D_2} C_L}{W_o} - \frac{\lambda_3}{qS} \qquad (57)$$

The system of differential equations and extremizing controls for the energy-heading angle boundary layer have been developed. The procedure for calculating the controls C_L, μ, η and the Valentine multipier is intricate due to the complex engine model and the many inequality constraints considered. The extremizing altitude must be found by a one-dimensional search. Care must be taken in doing this search to ensure that the global minimum in altitude is found precisely. The performance of the missile can now be examined.

CHAPTER 4. POINT PERFORMANCE

The solution has been set up for the energy-heading angle boundary layer. Recall that the problem of interest is to minimize the weighted sum of time elapsed and fuel consumed for a missile flying to a given point. This overall problem has been separated into three subproblems and are concentrating on the energy-heading angle trajectories which smoothly transition between different cruises. Before finding these transition trajectories, it is interesting to examine the maximum performance possible, independent of the outer cruise conditions.

However, it will be helpful to first discuss some concepts in the context of a general two state minimization problem. To find the extremal solution, consider minimizing the following variational Hamiltonian:

$$H = \lambda_{S_1}\dot{S}_1(S_1,S_2,u) + \lambda_{S_2}\dot{S}_2(S_1,S_2,u)$$

where S_1, S_2 = states

λ_{S_1}, λ_{S_2} = adjoint states

u = control

A typical plot of the pseudo-Hamiltonian in state-rate space for fixed values of the states is illustrated in Figure (4-1). In this *hodograph*, the controls are allowed to vary throughout their allowable ranges, forming the set of reachable state-rate points [15]. The contents of this set are dictated by the differential equations and constraints which describe the physics of the problem, and do not depend on the

adjoint variables. Superimposed on this plot are a representative set of constant pseudo-Hamiltonian lines. The slope of these lines is determined by the magnitude and signs chosen for the adjoint variables. In the case illustated in Figure (4-1), the objective is to increase both $\dot{S}_1$ and $\dot{S}_2$, so λ_{S_1} and λ_{S_2} are both negative. The lines have negative slope, with H decreasing up and to the right. The constant H line which is tangent to the hodograph is the *supporting hyperplane* and the tangent point and related controls correspond to the extremal solution (i.e. min H) at this instant.

If the magnitude of one of the multipliers is changed, the slope of the constant-H lines will shift and the associated extremal point will slide along the boundary of the hodograph. In this example, the constant H lines can range from vertical (λ_{S_2}=0, max $\dot{S}_1$) through a counterclockwise rotation to horizontal (λ_{S_1}=0, max $\dot{S}_2$).

In this study, several inequality constraints exist, as discussed in Chapter 2. The magnitudes used are: h_T equal to 0 feet for the terrain limit, the maximum load factor, $\bar{n}$, equalling 20 g's and a normalized maximum fuel flow rate of 1.05 units per second. Additionally, the throttle minimum is .275 and the maximum is 1.2. The aerodynamic limit on lift coefficient is a specified function of Mach number, but, as illustrated in Figure (A-7), its value is roughly unity. A consequence of this small value is that the altitudes of the corner-velocity locus are low in the performance envelope in Figures (2-1) and (2-2). The tight aerodynamic restriction on C_L also lowers the loft ceiling.

Review of Cruise Results

A brief review of the results of the cruise sub-problem is needed to motivate the choice of an interesting energy range. This is discussed in detail in [5]. The order reduction leading to the cruise-dash problem was briefly discussed in Chapter 2. From the state equations and the pseudo-Hamiltonian,

$$H = (-\lambda_x \cos\chi + \lambda_y \sin\chi)V + \lambda_F \eta\, Q_{STO}$$

$$\dot{x} = V \cos\chi$$

$$\dot{y} = V \sin\chi$$

$$\dot{W}_F = \eta\, Q_{STO}$$

From the Euler-Lagrange equations the adjoint variables are all constant, and from transversality conditions they are

$$\lambda_y = -\lambda_x \tan\chi$$

$$\lambda_F = \mu_F$$

$$\lambda_x = (\mu_t + \mu_F \eta Q_{STO})\frac{\cos\chi}{V}$$

Without loss of generality, set χ=0. By replacing energy with velocity

we can split the minimization into two nested parts. The result is:

$$\min_{h,V} H = \left[\min_{V} \mu_F \left(\min_{h} \eta Q_{STO} \right) - \lambda_x V \right]$$

Since the cruise states are ignorable, the cruise hodograph is independent of the values of the states. The lower boundary of the hodograph is illustrated in Figure(4-2) and several points on it correspond to classical cruise conditions. The lowest point on the curve, where fuel flow rate is minimum, is the endurance cruise. To the right is the point at which the boundary is tangent to the straight line going through the origin. This is the maximum range cruise, and for the fixed range problem at hand, it is the minimum-fuel cruise (μ_t=0). Finally, the right-most point on the boundary, where velocity is greatest, is the dash point (μ_F=0).

The cruise conditions spanned by $\mu_t \geq 0$ and $\mu_F \geq 0$ include the hodograph boundary between the latter two cruise points mentioned above. Starting with μ_t=0, the supporting hyperplane passes through the origin. As μ_t increases, the supporting hyperplane rotates counterclockwise and the extremizing point slides up and to the right on the curve, until the constant-H line is tangent at two points, V_1 and V_2. As μ_t increases further, the best velocity point jumps to V_2, rides around the hodograph briefly, and at V_3, must jump again to a higher cruise point, V_4. The details of these four interesting cruise points are tabulated in Table (4-1). From Figure (4-2), it appears that flight at an average velocity which lies between V_1 and V_2 would be accomplished most economically by time sharing between cruise at V_1

and cruise at V_2. The same would be true for flight at an average velocity between V_3 and V_4. Note that these results presuppose that altitude, energy and flight path angle can change "instantaneously."

Based on this analysis, the range of interesting energies considered in the following discussion will roughly span the slow cruise point through the fast cruise point,i.e. energies of 341,000 feet through 638,000 feet.

Fastest and Most Economical Climb

In this section the fastest climb, $\dot{E}_{max}$, and most fuel efficient climb, $\dot{E}_{EFF}$, are examined for the range of interesting energies. In this analysis, flight in the vertical plane is being considered, so $\mu=\dot{\mu}=0$. Since the peak climb performance is of interest, all considerations of range-rate are removed by setting $\bar{\lambda}_x$ and $\bar{\lambda}_y$ to zero. The pseudo-Hamiltonian reduces to:

$$H = \lambda_E \frac{V(T - D)}{W_o} + \bar{\lambda}_F \eta \, Q_{STO}$$

$$= \lambda_E \dot{E} + \bar{\lambda}_F \dot{W}_F$$

Hodographs for two representative energies are presented in Figures (4-3) and (4-4). In general, a hodograph for the energy-heading angle boundary layer is three-dimensional, with the axes being specific energy rate (or specific excess power), heading rate and the term

inherited from the cruise layer, $\{(-\bar{\lambda}_x \cos\chi + \bar{\lambda}_y \sin\chi)V + \bar{\lambda}_F \eta\, Q_{STO}\}$. In this case, $\chi=0$, and $\bar{\lambda}_x=\bar{\lambda}_y=0$ so the hodograph is reduced to two dimensions: Specific excess power versus fuel flow rate.

Because of the gap in allowable throttle settings, these hodographs consist of two disconnected regions. The presence of this nonconvexity raises the possibility of chattering throttle for some problems. The left-hand line of points corresponds to the engine-off conditions with the highest point being the minimum power required. The right hand part of the hodograph includes all engine-on conditions. For low energies, the maximum fuel flow limit restricts the range of throttles which can be reached.

For fastest climb, $\bar{\lambda}_F=0$ and the supporting hyperplane is horizontal at the largest $\dot{E}$ possible. The problem of finding the most fuel efficient energy rate can be recast as follows:

$$\max \frac{\partial E}{\partial W_F} = \max \frac{\dot{E}}{\dot{W}_F}$$

In other words, the supporting hyperplane will be the line passing through the origin which is tangent to the upper boundary of the hodograph.

For specific energies of 260 kft and less, the upper boundary of the hodograph is concave and the tangent points for max $\partial E/\partial W_F$ and max $\dot{E}$ coincide. Above 260 kft of specific energy, the two tangent points are distinct as can be seen in Figure (4-4).

Over the range of energies relevant to this problem, $\dot{E}_{max}$ and $\dot{E}_{EFF}$ vary over a large range of magnitudes, as illustrated in Figure (4-5).

For the lower energies, the economy climb rate is considerably smaller than the energy climb rate, with only a minimal improvement in fuel efficiency. At each value of energy, the altitude for economy climb is somewhat higher than that for the energy climb. Over the higher energies of interest, the achieved $\dot{E}$ and $\partial E/\partial W_F$ values and the corresponding altitude curves lay quite close together (Figures 4-5, 4-6, 4-8). The throttle settings, however, are quite different (Figure 4-7). This is a consequence of the complex engine model, where for values of throttle near unity, large changes in throttle can result in only slight changes in fuel flow rate, as illustrated in Figure (A-14).

Fastest Turn

Two types of maximum turn are of interest here, fastest instantaneous turn and fastest sustainable turn. In the first case, the objective is to find the maximum turn rate, regardless of what happens to the other states. In the second case, $\dot{E}$ is required to be zero, allowing the missile to turn "indefinitely."

The analysis is similar to that of the previous section. In this case, $\bar{\lambda}_F=\bar{\lambda}_x=\bar{\lambda}_y=0$, and

$$H = \lambda_E \frac{V(T - D)}{W_o} + \lambda_\chi \frac{g \tan\mu}{W_o V}$$

$$= \lambda_E \dot{E} + \lambda_\chi \dot{\chi}$$

Representative hodographs are presented in Figures (4-9) through

(4-11). Note that, because these hodographs are symmetric about the $\dot{E}$ axis, only the top halves, corresponding to positive turn rates and negative values of λ_χ, are shown. The left region of each hodograph corresponds to engine off. To understand the structure of the right region, it is useful to visualize a third axis, altitude, normal to the page. At at each altitude, varying C_L and η forms a sheet. The layering of these sheets forms a "mountain" from the low altitude limit to the loft ceiling. For a fixed altitude, increasing the throttle for fixed C_L increases the energy rate. As C_L increases, more lift is available for turning and heading rate becomes larger. Finally, for increasing altitude, the dynamic pressure drops, reducing the maximum possible turn rate and the "sheet" shrinks in size until the loft ceiling is reached, where there is only a small line of energy rates at zero turn which can be reached.

The left boundary in each of these turn hodographs is concave. If it were desirable to lose energy rapidly, without a net change in heading angle, it appears that the best strategy would be to turn the engine off and fly at minimum altitude, "chattering" [15] between $+\dot{\chi}_{max}$ and $-\dot{\chi}_{max}$. To examine this, it would be necessary to modify the differential equations so as to relax the problem, yielding a new problem which is more complex, but which does not have this non-convex region.

For $\lambda_E \leq 0$ and $\lambda_\chi \leq 0$, the boundary of interest is on the right. When $\lambda_\chi = 0$, the constant Hamiltonian lines are vertical, which corresponds to the $\dot{E}_{max}$ solution of the previous section. As $|\lambda_\chi|$ increases, the lines rotate counterclockwise and the extremal points migrate up the

border. Once the upper right corner of the hodograph is reached, increasing $|\lambda_\chi|$ further has no effect on the solution of the problem; the supporting hyperplane simply pivots about that point. Finally, for $\lambda_E=0$ the constant Hamiltonian lines are horizontal and the solution becomes independent of E. If λ_E remains zero, the solution may include a singular arc.

Figures (4-12) and (4-13) illustrate the maximum instantaneous and maximum sustainable turn rates and the corresponding altitudes. Because the extremizing altitude increases rapidly with energy, the largest possible turn rate drops rapidly. For low energies, the sustainable turn rate is smaller than the maximum instantaneous turn rate. This is clear after examining hodograph in Figure(4-9), where the $\dot{E}=0$ axis intersects below the maximum turn rate. From this, to achieve the maximum turn rate, it is necessary to sacrifice energy. However, for hodographs at energies above 290 kft, the $\dot{E}=0$ axis passes through the $\dot{\chi}_{max}$ boundary and the two turn rates are the same. This unusual result is a consequence of the low constraint on lift coefficient and the high thrust available (Figure 2-1).

For the energies of interest here, the two turn rates are the same and they peak at less than five degrees per second. This fairly small number is due to the fact that the turn rate is inversely proportional to speed and high speeds are being considered.

Also interesting is the fact that for these energies, $\dot{\chi}_{max}$ is independent of $\dot{E}$ in each hodograph. This is because the corner-velocity locus is out of reach, as is clear from a slight recasting of the heading angle equation:

$$\dot{\chi}_{max} = \frac{g \tan\mu_{max}}{V} = \frac{g\sqrt{a^2-1}}{V} \qquad \text{where,} \quad a = \frac{\bar{C}_L q S}{W_0}$$

The combination of $\bar{C}_L$ and h for maximum lift is unique. The only remaining control is η, which affects $\dot{E}$ but not $\dot{\chi}$.

Since maximum turn rate increases with decreasing energy, a good strategy for fast turns through large angles would seem to be to decrease energy as rapidly as possible and to remain at maximum bank angle until near the desired heading. This would entail λ_E=0 for a finite length of time, resulting in a reduced order arc.

CHAPTER 5. TRANSITIONS TO CRUISE

In Chapter 4 the cruise performance of the missile was discussed. It was shown that the problem of minimizing a weighted sum of time and fuel can have an unanticipated complexity. In order to fly optimally and maintain a given average speed it may be necessary to initially cruise at one flight condition and then transition to a second cruise condition.

The problem is now considered in which the missile, while in flight, is directed to a new heading. This situation would arise if, for example, an updated estimate of the target's range and heading were transmitted to the missile. Since the required change in heading angle would likely be accompanied by a change in average speed, it is appropriate to study maneuvers in which both energy and heading angle change (Figure (5-1)).

In this study it is convenient to use a coordinate system in which the x-axis is parallel to the desired final course (Figure (5-2)). Since the incoming heading is specified, and generally nonzero, the initial value of the y-coordinate depends on when the maneuver is initiated. The change in the y-coordinate during the optimal maneuver is controlled by the constant muliplier $\bar{\lambda}_y$. See Equation (34). Note that since the y-coordinate does not appear on the right-hand side of any state equation, the constraint on the change in y is of the isoperimetric type. In the present study, only the natural boundary condition, $\bar{\lambda}_y=0$, is considered [2, pp.56 and 90].

To produce flight ending in a specified $y(t_f)=y_f$ path, the change

in y during this "natural" maneuver can be computed and, from that, the place at which to initiate the maneuver can easily be found. If the missile receives the command to maneuver before it has flown through the point to initiate the "natural" maneuver, the procedure would be to maintain current course until that point is reached, then maneuver. If, however, this point has been overflown, then the problem with the isoperimetric constraint active, i.e. $\bar{\lambda}_y \neq 0$, is appropiate. Thus, the $\bar{\lambda}_y = 0$ is an important member of the family of energy-heading maneuvers, but not the only one of interest.

Approach

In Figure (5-2) the states, costates and cruise multipliers appropriate to the trajectory before, at the start of, and at the end of the maneuver are illustrated. At the start of the maneuver, t_0, the states correspond to those at t_{-1} and the cruise multipliers correspond to those of the final cruise at t_f. The initial values of the energy and heading costates must be chosen to place the missile on the proper trajectory. A consequence of the change in costates and cruise multipliers at t_0 is that the resulting trajectories will have a "kink" in the state time histories.

Finding the proper initial values of λ_E and λ_χ is complicated by the fact that the desired trajectories must fair asymptotically into the final cruise. For this to happen the choices of initial values must be *precisely* correct. This is because of the structure of the linearized state-adjoint system at an equilibrium point. As developed

in [11], the characteristic values occur not only in complex conjugate pairs, but in real pairs of the form $\pm a \pm ib$. Thus, for every stable mode there is an unstable mode.

The only way to manage this apparently intractable structure is to suppress the unstable modes by ensuring that the trajectory approaches this unstable equilibrium exclusively along the stable modes. Otherwise, the trajectory will approach the equilibrium point only to shoot off in the unstable direction before reaching its goal.

The approach taken is to "start" computation of a trajectory at conditions which are perturbed slightly from the final cruise, and then integrate the trajectory equations in negative time. These "initial" perturbations are chosen to be along the stable characteristic vectors. By proper choice of these perturbations, different trajectories are traced out. When following this procedure, the nonlinear system is assumed to be closely approximated by a linear stable surface. When the perturbation is small enough, the nonlinear and linarized systems are nearly identical in behavior. This assures that in positive time the perturbed state will decay to the equilibrium value. A secondary advantage of this approach is that these trajectories, which in principle, take an infinitely long time to complete, are reduced to a managable length of time.

In the discussion which follows, references to the computations of the trajectory in negative time are placed in quotes, as in the paragraph above, to distinguish from the positive flow of time in which the flight would actually take place.

Results

The third cruise point in Table (4-1) was chosen as the final condition. The characteristic structure of the energy-heading angle system about this point was examined numerically using central difference approximation. First the system was scaled so that the values of the states and costates would be the same order of magnitude. Then the size of the difference in each state was independently adjusted to yield results with consistent forward and backward differences.

In the linear system, the energy and heading transients are uncoupled:

$$\dot{\underline{x}} = [A]\ \underline{x}$$

$$\underline{x} = \{E\ (ft),\ \lambda_E(s/ft),\ \chi(rad),\ \lambda_\chi(s/rad)\}^T$$

$$[A] = \begin{Bmatrix} -.0035452 & -.257823\text{x}10^7 & 0.0 & 0.0 \\ -.23323\text{x}10^{-10} & .0035504 & 0.0 & 0.0 \\ 0.0 & 0.0 & 0.0 & -.0013760 \\ 0.0 & 0.0 & -.0381268 & 0.0 \end{Bmatrix}$$

The four characteristic values and associated characteristic vectors are fortunately real:

$$\sigma_1 = -.008525032\ s^{-1} \qquad u_1 = \begin{Bmatrix} 0.981853 \times 10^5 \\ 0.189643 \times 10^{-3} \\ 0. \\ 0. \end{Bmatrix}$$

$$\sigma_2 = .008530157\ s^{-1} \qquad u_2 = \begin{Bmatrix} -0.905595 \times 10^5 \\ 0.424144 \times 10^{-3} \\ 0. \\ 0. \end{Bmatrix}$$

$$\sigma_3 = -.007243215\ s^{-1} \qquad u_3 = \begin{Bmatrix} 0. \\ 0. \\ 0.1866388 \\ 0.9824286 \end{Bmatrix}$$

$$\sigma_4 = .007243215\ s^{-1} \qquad u_4 = \begin{Bmatrix} 0. \\ 0. \\ -0.1866388 \\ 0.9824286 \end{Bmatrix}$$

The independence of the heading transient from perturbations in energy was expected; this is globally true because the family of extremals admits purely vertical plane maneuvers. That the *energy* transient would even locally be independent of perturbations in heading was a surprise.

To create the trajectories, the "starting" conditions are perturbed from equilibrium as follows:

$$\underline{x} = \underline{x}_e + a\ \underline{u}_1 + 0\ \underline{u}_2 + b\ \underline{u}_3 + 0\ \underline{u}_4$$

The magnitudes of "a" and "b" determine how far from the equilibrium point execution "starts": too far and the range of the linearization has been exceeded, too close and execution lasts a very long time. The importance of not starting too close to equilibrium is clear from the

small magnitudes of the characteristic values. The associated times to double amplitude (in negative time) are nearly 100 seconds.

Energy : $t_{1/2}$ = 81.3 sec

Heading: $t_{1/2}$ = 95.7 sec

The perturbations used were smaller than the magnitudes of the differences used to study the linearized system. The value of the ratio (a/b) determines which trajectory will be traced out. In the study, further restrictions were placed on the values the two multipliers may take. First, "a" must not result in λ_E becoming positive at any time. Second, because of symmetry, only negative values of "b", corresponding to turns through a positive change in heading were examined.

The resulting family of trajectories which fair smoothly into the cruise point is illustrated in Figures (5-3) through (5-11). Note that Figure (5-8) fits in the upper right quarter of the performance envelope of Figure (2-1). Also indicated on these figures are the energies of the four cruise points from Table (4-1). To generate the family of curves (in negative time), "a" is 10^{-3}, 0, or -10^{-3} and "b" ranges from 0 to -1.

For the case of decreasing energy to cruise with no turn (a>0, b=0; curve A in Figure (5-3)), the strategy is to lose energy rapidly, early in the trajectory. At high energy, the trajectory rides the low altitude limit briefly, then the throttle drops back and the lift coefficient increases rapidly to $\bar{C}_L$ as the missile climbs to the loft

ceiling (Figures (5-5), (5-6) and (5-8)). The resulting high drag combined with the abrupt drop in thrust causes the energy to drop rapidly. As the trajectory rides the loft ceiling locus, the lift coefficient and dynamic pressure grow, causing drag to continue to increase. However, thrust is increasing due to the drop in altitude, even though the throttle is nearly constant (see Figure (A-12)). The rate of energy loss decreases. In the vicinity of the equilibrium cruise point, the trajectory leaves the loft ceiling and the lift coefficient drops slightly so that drag is nearly constant at the cruise value. The throttle increases slightly to result in equilibrium flight.

For turns with energy decreasing to the equilibrium cruise ($a \geq 0$, $b < 0$; Region II in Figure (5-3)), the trajectories are similar to the one just described. Early (in forward time) in trajectory B there is a segment where the low altitude and maximum lift coefficient constraints are simultaneously active. As can be seen by comparing Figures (5-9) and (4-12), this segment of the trajectory corresponds to the fastest turn conditions described in Chapter 4. Again, the strategy is to accomplish most of the maneuver early in the trajectory. After a brief time at maximum lift coefficient, the trajectory is much like the no-turn case, except that the loft ceiling is now out of reach due to a slight bank angle. In trajectories C through E, heavier emphasis on turning causes the trajectories to spend more time on the fast turn locus and to reach lower altitudes. Note that trajectory E ($a=0$) approaches the cruise point along a constant energy line, confirming the structure of the linear system noted earlier.

These trajectories start out at either the low throttle or zero throttle settings (Figure (5-6)). Late in the study a slight nonconvexity was found in the functional fit of thrust versus throttle, leading to jumps in throttle from internal values to the lower bound. The portions of the trajectories for which the Hamiltonian varies by less than one percent are included. However, these segments must be viewed with caution since the throttle-jump indicates a nonconvexity in the hodograph figure. To be on firm thoretical ground the problem should be relaxed; this introduces a singular throttle possibility which was not examined in this study.

The trajectories of region II include energy gain to the cruise point with no turn ($a<0$, $b=0$) and with moderate turn ($a<0$, $b<0$ and small). These trajectories appear to have two phases. Referring again to forward time, the initial phase is at energies lower than the slow cruise energy of Table (4-1). Here the altitude increases rapidly accompanied by a rapid increase in lift coefficient and a decrease in throttle. In the second phase, the turn rate is nearly constant with energy and more moderate than in the first phase (Figure (5-9)). Up to around 400,000 feet of energy, the altitude and lift coefficient drop while throttle grows. For the rest of the flight, the altitude, lift coefficient and throttle move smoothly to their cruise values.

The trajectories in region III ($a<0$, $b<0$ and larger in Figure (5-3)) still approach the equilibrium point from lower energy, but they have a fundamental change in character from the curves of region II. They start out on the low altitude constraint near the loft ceiling and then, as illustated in Figures (5-8) and (5-9), they drop several tens

of thousands of feet in altitude along $h=\bar{h}$ with $C_L=\bar{C}_L$ and $\dot{\chi}=\dot{\chi}_{max}$. The missile then leaves the low altitude limit and, still turning rapidly, loses more energy while climbing to a point where it finally approaches the cruise point much like the trajectories of Region II. This strategy allows the missile to change heading by as much as 100 degrees.

In region III of Figure 5-3, simple coverage of the state space is lost when trajectory J crosses curves H and I. All the trajectories are still extremal, but now some are only locally minimal. Evaluation of the cost to fly along J and along I from point 1 on Figure (5-3) to equilibrium reveals that path J takes longer and consumes more fuel. The same is true for trajectories H and J from point 2 on the same figures. Clearly, path J is optimal only from a point to the left of point 1. Determining the precise point at which J loses optimality would require application of second order tests such as the Jacobi necessary condition [3, pg. 181]. Also of interest is region IV and the boundary between regions II and III. The boundary between the two regions may well be a trajectory, or separatrix [2, pg. 15], connecting a steady state turn at the slow cruise energy to the zero-turn final cruise. The "splitting" in character is also apparent in a much milder form about a point at the fast cruise energy in Figures (5-5) and (5-6). The boundary between regions II and III leads to region IV, from which the cruise point cannot be reached. This empty region may well be a symptom of a nonconvex hodograph in $E - \chi - (\bar{\lambda}_x V\cos\chi + \lambda_F \eta Q S T O)$ space. This conjecture is strengthened by the fact that, in Figure (5-6), the region II throttles are all greater than

η_{min}, but those in region III include time at η_{min} and at η=0. To reach the final cruise from points in region IV may require throttle settings between η_{min} and zero. For this missile, this would be possible only by chattering between η_{min} and zero. If this chattering were allowed, the trajectories in region III might well become less extreme. To model this would entail "relaxing" the problem and introducing an additional throttle-type control. In this study, no provision was made for this type of behavior.

A family of trajectories which fair asymptotically into cruise has been presented. Since they are asymptotic, the times of flight are large (on the order of 800 to 1000 seconds), over half of which is spent within a few percent of cruise. These extremal paths include energy changes as large as 200,000 ft and heading changes of up to 90 degrees. To reach the final cruise from a much lower energy and a large heading error appears to require chattering throttle.

CHAPTER 6. SUMMARY

A reduced order model of the energy and heading dynamics for a scramjet missile has been formulated. Using this model, the extreme turning and climbing capability of the missile has been examined for the range of energies over which the missile can cruise efficiently. Little penalty is paid for climbing at the energy climb rate rather than at the fuel efficient rate. However, for long range flights, the small improvement in the energy-to-fuel ratio may become significant. The missile's peak energy climb, fuel efficient climb and peak turn rates are much larger at the lower energies, indicating that it would be impractical to attempt extreme maneuvers at high energies.

Past work on the reduced order cruise-dash model was reviewed with the result that there are four fuel-efficient cruise conditions. To fly most efficiently at average velocities between these cruise points requires time-sharing between the bracketing efficient cruise-points.

A family of energy-heading trajectories was then constructed which fair smoothly into one of the efficient cruise points. In general, the strategy in these trajectories is to accomplish the bulk of the maneuver early in the trajectory. When a large change in heading is necessary, the missile turns along the peak turn rate locus.

It was also discovered that there is a region consisting mostly of low energies and large heading angles from which the desired equilibrium point cannot be reached, as well as "double-coverage" of a region of large initial heading angles. It would be interesting to examine both of these phenomena in more detail, and to see what effect

provision of throttle chattering between the minimum setting and engine-off would have on them.

In this study a family of energy turns has been developed where only final heading and energy are specified; additional considerations of getting on a *particular* final path would be addressed by initiating the maneuver at the proper point in the original trajectory. A reasonable extension of this work would be to consider the class of trajectories where a desired final flight path is obtained by considering the isoperimetric constraint on the y-coordinate. With this problem solved, strategies addressing scenarios where command update arrives after the time to initate the "natural" type of maneuver could be implemented. This would expand the capability of the missile to adapt to updated mission requirements.

REFERENCES

1. Ardema, M. D., "Singular Perturbations In Flight Mechanics," NASA Technical Memorandum X-62,380, 1974, Second Revision 1977.

2. Bergé, P., Pomeau, Y. and Vidal, C., Order Within Chaos: Towards a Deterministic Approach to Turbulence, John Wiley and Sons, Inc., 1984.

3. Bryson, A. E. and Ho, Y. C., Applied Optimal Control, Revised Printing, Hemisphere Publishing Co., 1975.

4. Calise, A. J. and Moerder, D. D., "Singular Perturbation Techniques for Real Time Aircraft Trajectory Optimization and Control", NASA CR-3597, 1982.

5. Chichka, D. F., "Cruise-Dash Optimization Applied To an Air-Breathing Missile," Masters Thesis, VPI&SU, December, 1985.

6. Cliff, E. M., Kelley, H. J. and Lefton, L., "Thrust-Vectored Energy Turns," Automatica, Vol. 18, No. 5, 1982.

7. Cliff, E. M., Kelley, H. J. and Lutze, F. H., "A Study of Systems Optimization Applied to Surface-to-Air Missile Operations," Report to NSWC, VPI&SU, March 1985.

8. Hedrick, J. K. and Bryson A. E. Jr., "Three-Dimensional, Minimum Fuel Turns for a Supersonic Aircraft," AIAA Journal of Aircraft, Vol. 9, No. 1, March 1972.

9. Hestenes, M. R., Calculus of Variations and Optimal Control Theory, John Wiley and Sons, Inc., 1966.

10. Kaiser, F., "Der Steigflug mit Strahlflugzeugen; Teilbericht 1: Bahnngeschwindigkeit für Besten Steigens," Versuchs-Bericht Nr. 262 02 L44, Messerschmitt A. G., Lechfeld, May 1, 1944. Translated into English as R.T.P./T.I.B. Translation No. G.D.C./15/148T, Ministry of Supply (U. K.).

11. Kelley, H. J., "Aircraft Maneuver Optimization By Reduced Order Approximation," Control and Dynamic Systems, Vol. 10, C. T. Leondes, ed., Academic Press, 1973, pp. 131-178.

12. Leitmann, G., An Introduction To Optimal Control, McGraw-Hill Book Co., 1966.

13. Shankar, U. J., "Singular Perturbation Analysis Of Climb-Cruise-Dash Optimization," Masters Thesis, VPI&SU, May 1985.

14. Shinar, J., Farber, N. and Negrin, M., "A Three-Dimensional Air Combat Game Analysis of Forced Singular Perturbations," AIAA paper 82-1327, August 1982.

15. Vinh, N. X., Optimal Trajectories in Atmospheric Flight, Elsevier Scientific Publishing Co., 1981.

APPENDIX - AERODYNAMIC AND PROPULSIVE MODELS

The data describing the atmospheric properties, the missile's aerodynamics and the propulsion are from [6] and are stored as a set of arrays. These are interpolated with cubic splines and, for two dimensional arrays, with spline-lattices. For those quantities which are functions of three variables, a low order polynomial fit was used to capture the dependence with respect to the simplest variable. By using splines to interpolate the data, the resulting interpolated curves are guaranteed to be continuous with continuous slope. It is very risky to attempt to extrapolate using these fits because, without data points to control the functions, the resulting curves have wild tails.

Care must be taken in evaluating the derivatives from splines. The derivative resulting directly from the splines is the same as would come from reading the slope off the corresponding plot. However, in several cases one of the "independent" variables is itself a function of another independent variable. For example, drag coefficient is tabulated as a function of Mach number and altitude. But since all derivatives are evaluated at constant energy, and $M = \frac{V}{a} = \frac{2g(E-h)}{a}$, the full derivative of C_D with respect to altitude at constant energy is:

$$\frac{\partial C_D}{\partial h} = C_{D_h} + C_{D_M} \frac{\partial M}{\partial h}$$

Atmosphere

Sonic speed and the natural log of atmospheric density are tabulated as functions of altitude. The data, interpolated by cubic splines, are illustrated in Figures (A-1) and (A-2).

Aerodynamics

Drag is a function of dynamic pressure and two drag coefficients, one due to the body, the other due to the engine inlet.

$$D = \frac{1}{2} \rho V^2 S(C_D + C_{xe})$$

The body drag coefficient is tabulated as a function of Mach number, altitude and lift coefficient, and is interpolated with respect to Mach and altitude with a cubic spline-lattice and with respect to lift coefficient using a quadratic polynomial.

$$C_D = C_{D_0}(M,h) + C_{D_2}(M,h)C_L^2$$

The inlet drag is a tabular function of Mach number, and is interpolated using a cubic spline.

$$C_{xe} = C_{xe}(M)$$

The maximum lift coefficient is also a tabular function of Mach number.

The values correspond to a maximum angle of attack of eight degrees. This low limit was imposed because of unrealistic data at higher angles of attack. For this missile, however, the peak angle of attack would generally be fairly small because of the need to avoid engine stall.

Typical aerodynamic plots are presented in Figures (A-3) through (A-7).

Engine

The model for this missile's ramjet engine is unusually complex, particularly in its cubic dependence on the throttle. A consequence of this is that the maximum thrust may occur at a throttle setting which is less than the maximum. Figures (A-8) through (A-14) illustrate typical engine-on curves.

$$T = \dot{W}_F I_{sp} e$$

T = thrust

$\dot{W}_F$ = fuel flow rate

I_{sp} = specific impulse

e = propulsive efficiency (constant)

$$\dot{W}_F = \eta Q_{STO}$$

η = throttle

Q_{STO} = stoichiometric fuel flow rate

$$Q_{STO} = F_A \dot{W}_A$$

F_A = fuel to air ratio for stoichiometric combustion (constant)

$\dot{W}_A$ = flow rate of intake air

$$\dot{W}_A = \rho V S_e g \frac{A_o}{A_i}$$

S_e = engine characteristic area

$\frac{A_o}{A_i}$ = engine capture ratio, function of Mach number

g = acceleration due to gravity (constant)

$$I_{sp} = w_o(M,h)+w_1(M,h)\eta+w_2(M,h)\eta^2$$

When the engine is off, the internal flow is an additional source of drag (Figure (A-15)). It is treated as a negative "thrust" and is evaluated using a cubic spline.

$$T = C_T(M,h) q S_e$$

C_T = engine-off drag

$$I_{sp} = Q_{STO} = 0$$

Table 4-1 Cruise Points

	1 Slow	2 Slow middle	3 Fast middle	4 Fast
V (ft/s)	4,084.4	5,104.7	5,132.6	5,922.5
h (ft)	81,794.5	89,727.0	89,902.2	93,220.1
$\dot{W}_F$(norm.)	.062175	.084366	.084983	.10271
η	.47389	.663334	.66855	.77294
$\bar{\lambda}_x$(s/ft)	.0008159288	.0008159288	.0007428363	.0007428363
$\bar{\lambda}_F$(s/lb)	5.6273742	5.6273742	4.9645493	4.9645493
E (ft)	341,226.	494,681.	499,294.	638,319.
λ_E(s/ft)	-.001622910	-.001740436	-.001541164	-.001865855

For all conditions: $\mu_t = 1.$

$\bar{\lambda}_y = 0.$

$\chi = 0.$

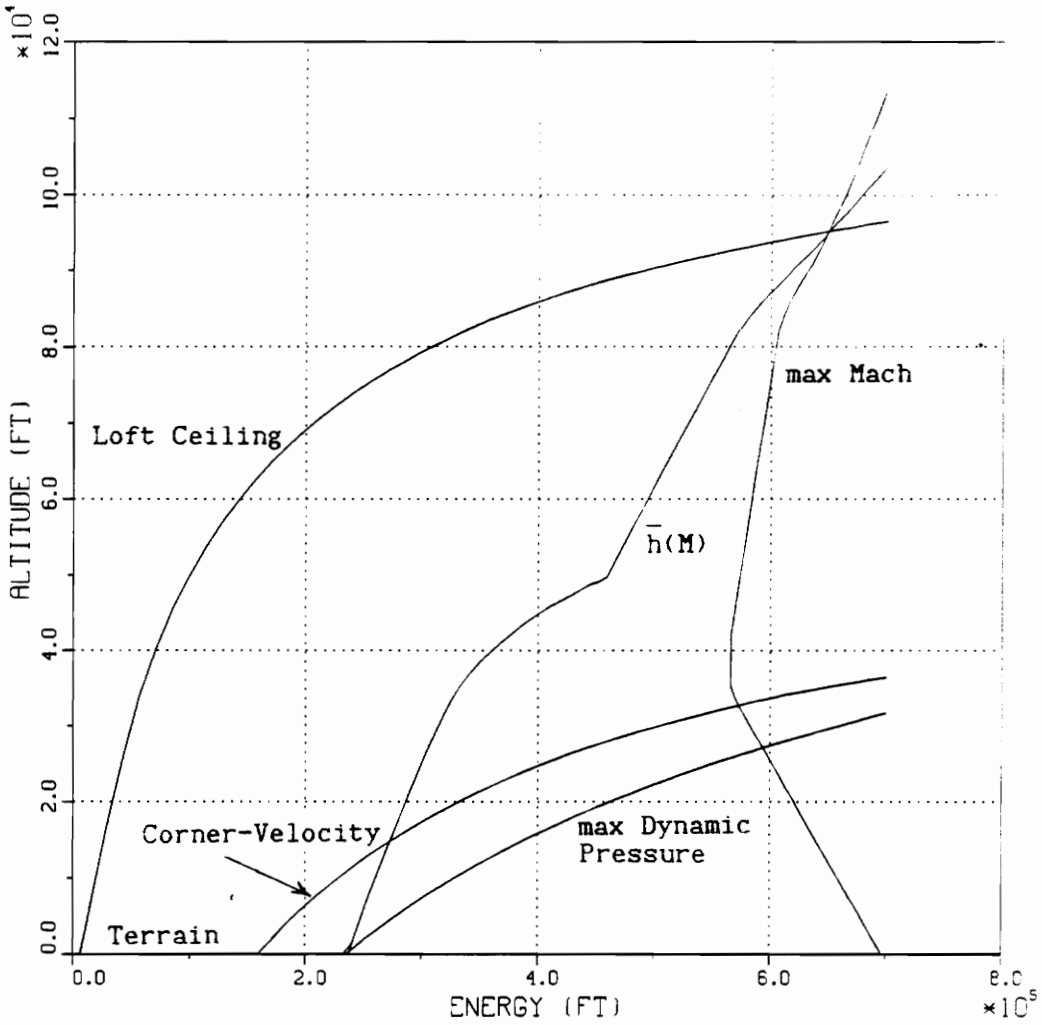

Figure 2-1. Performance Envelope: h vs. E

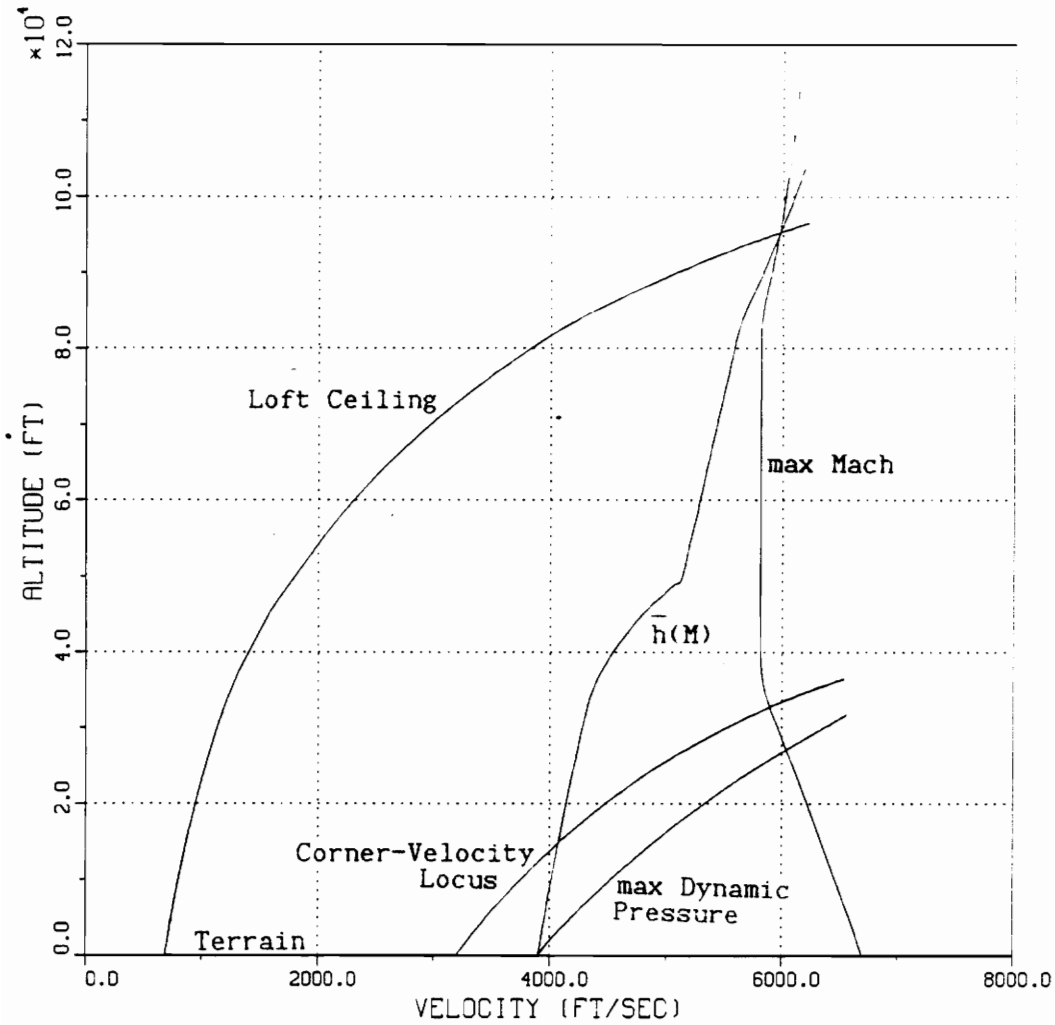

Figure 2-2. Performance Envelope: h vs. V

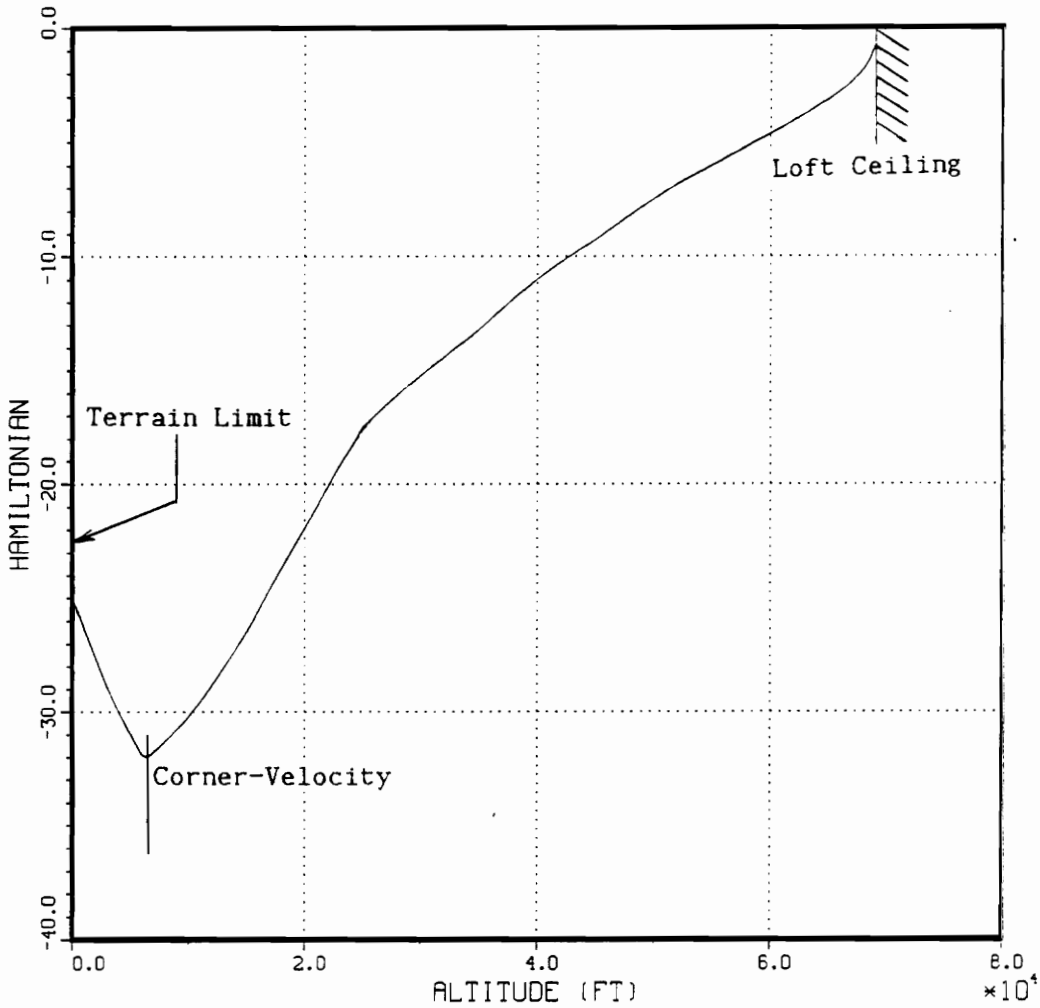

Figure 3-1. Typical Hamiltonian vs. Altitude

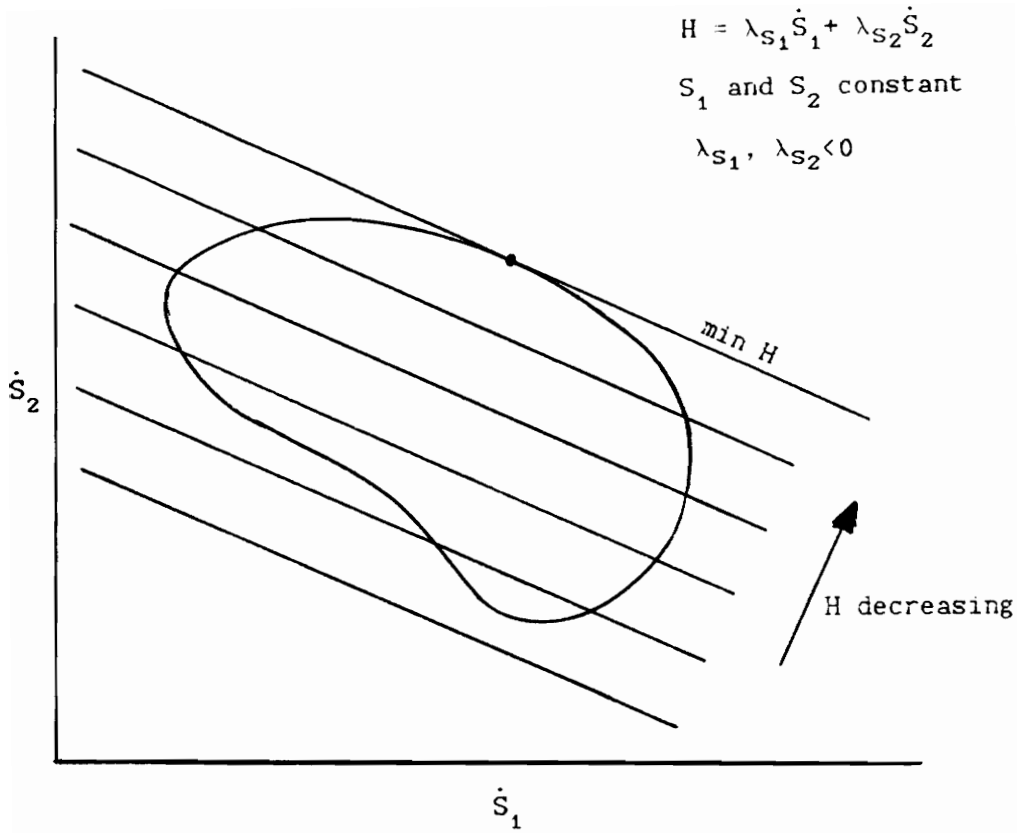

Figure 4-1. Generic Hodograph

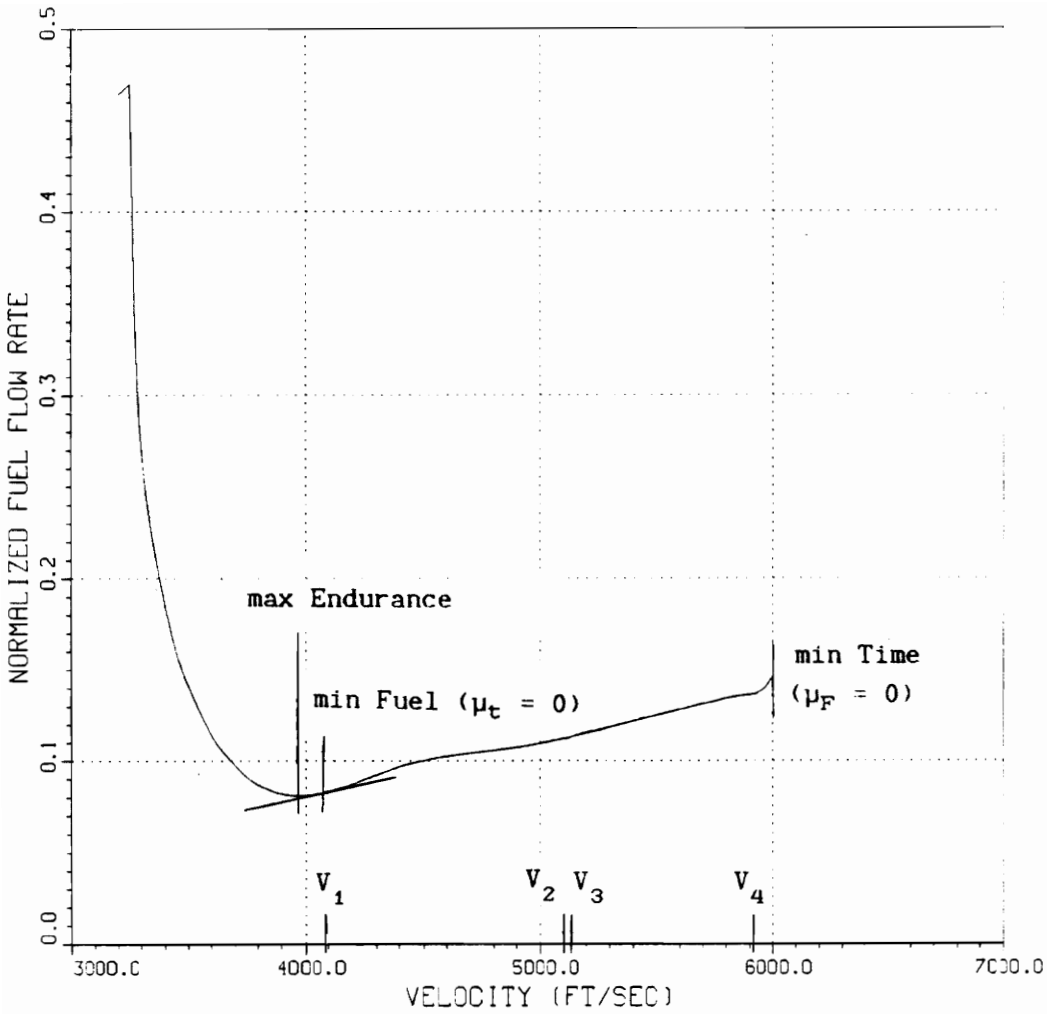

Figure 4-2. Cruise Hodograph

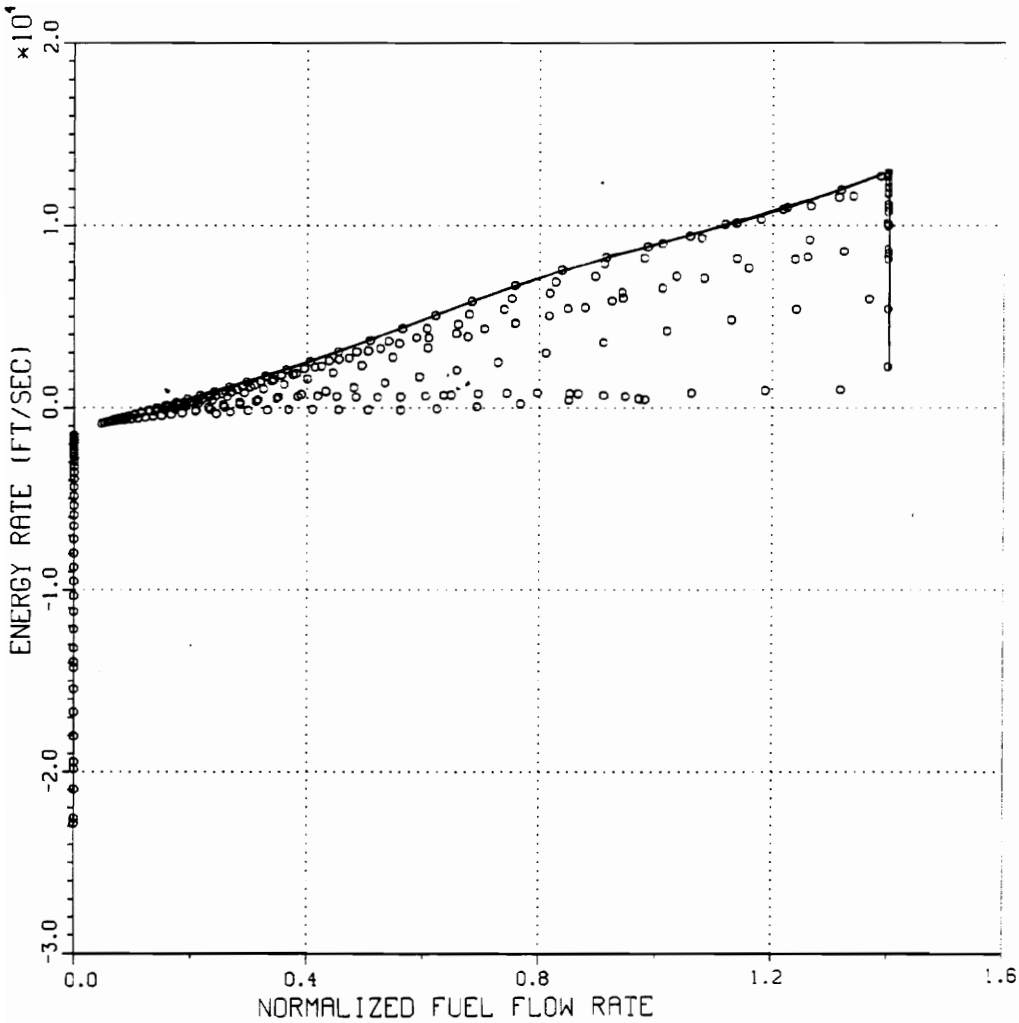

Figure 4-3. Energy-Fuel Flow Hodograph, E = 260 kft.

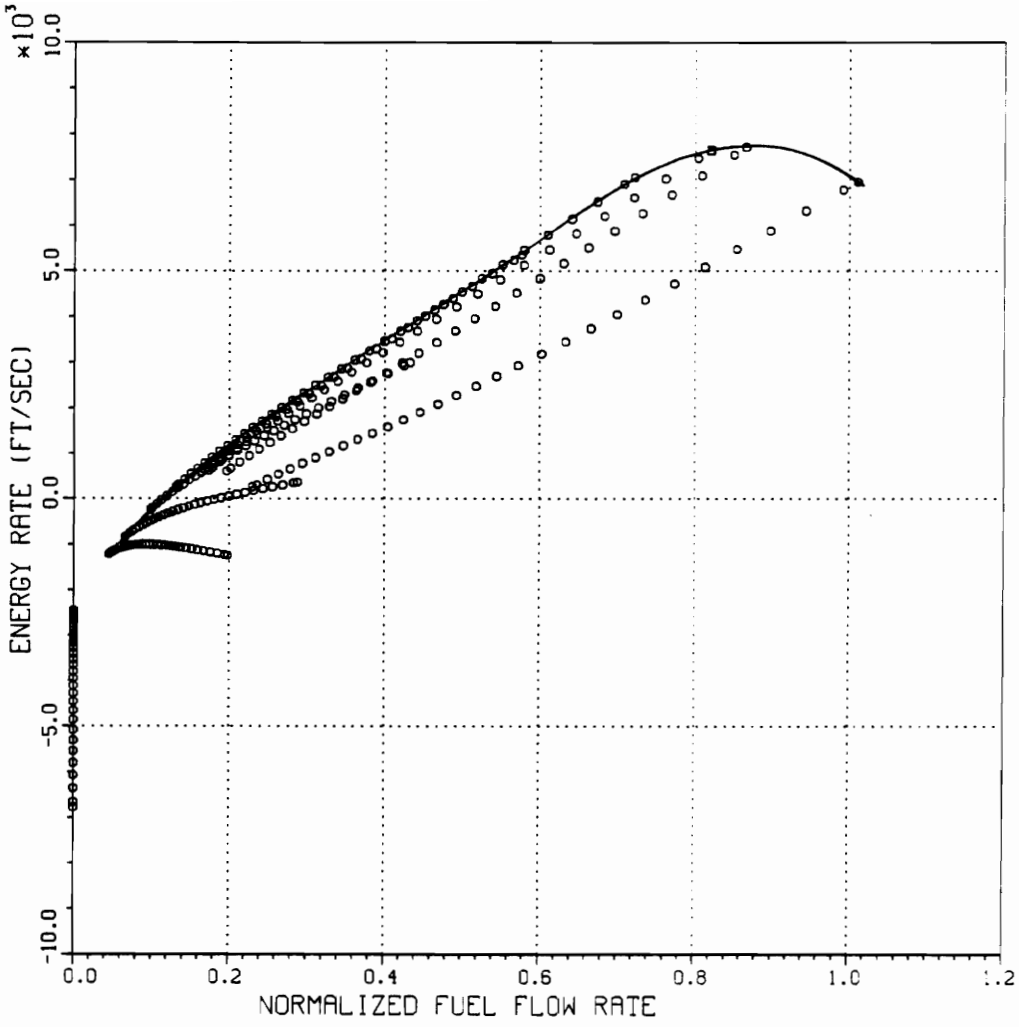

Figure 4-4. Energy-Fuel Flow Hodograph, E = 500 kft.

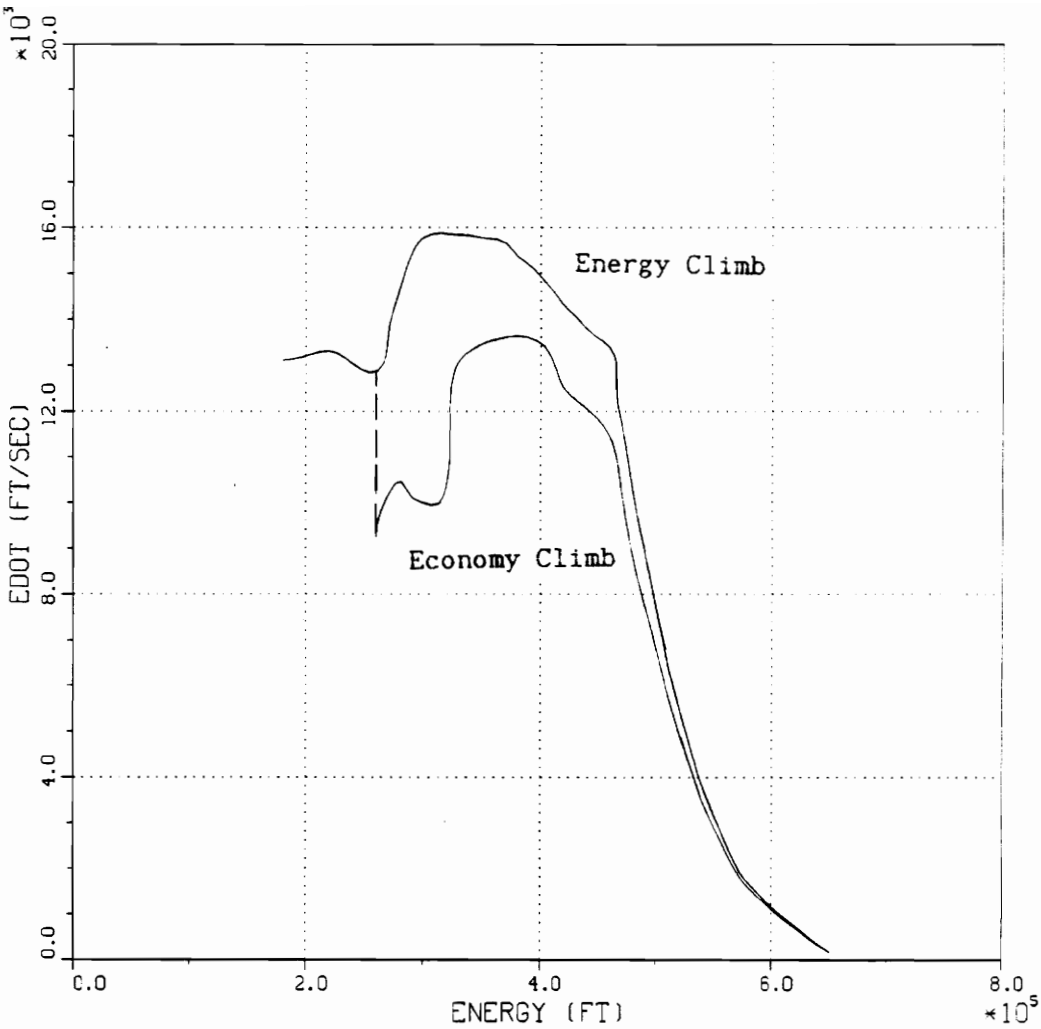

Figure 4-5. Fastest and Most Economical Energy Rates

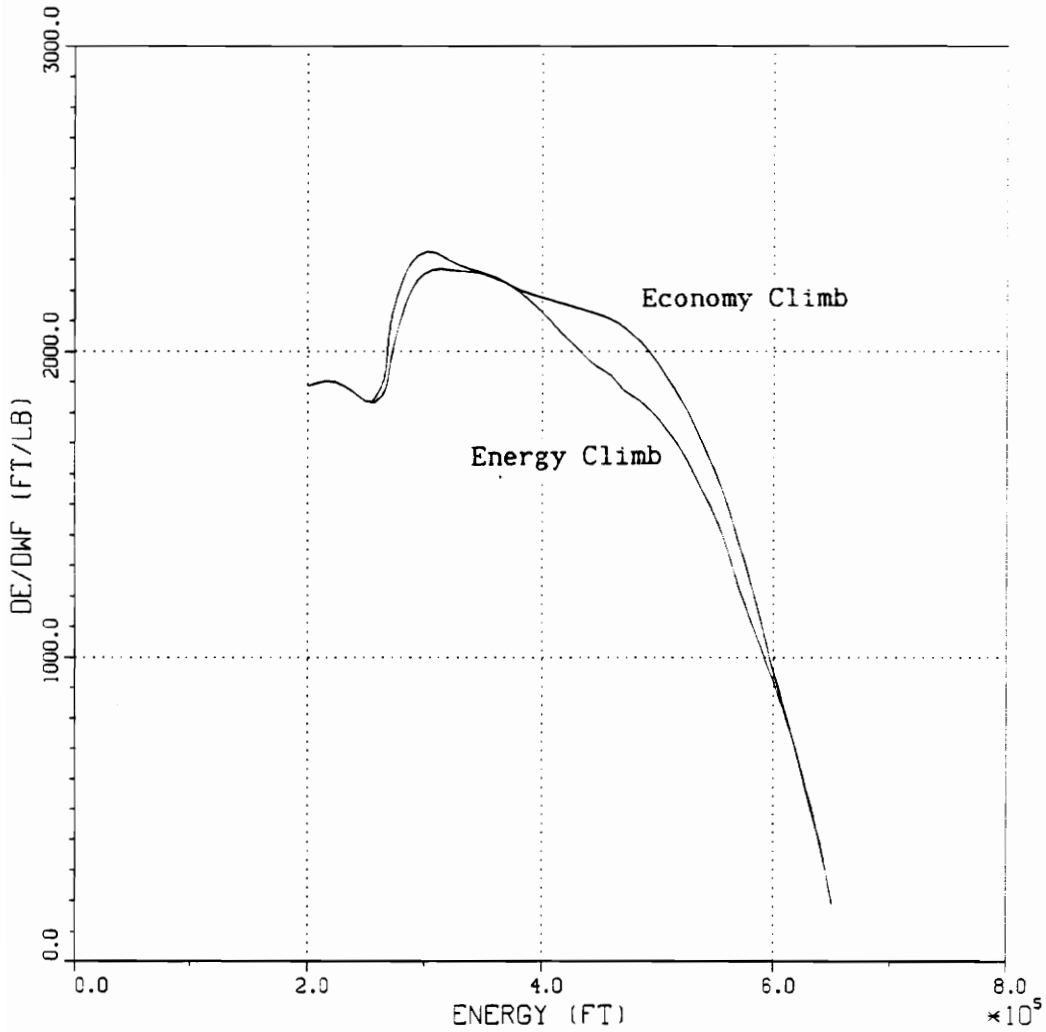

Figure 4-6. Energy per Pound of Fuel

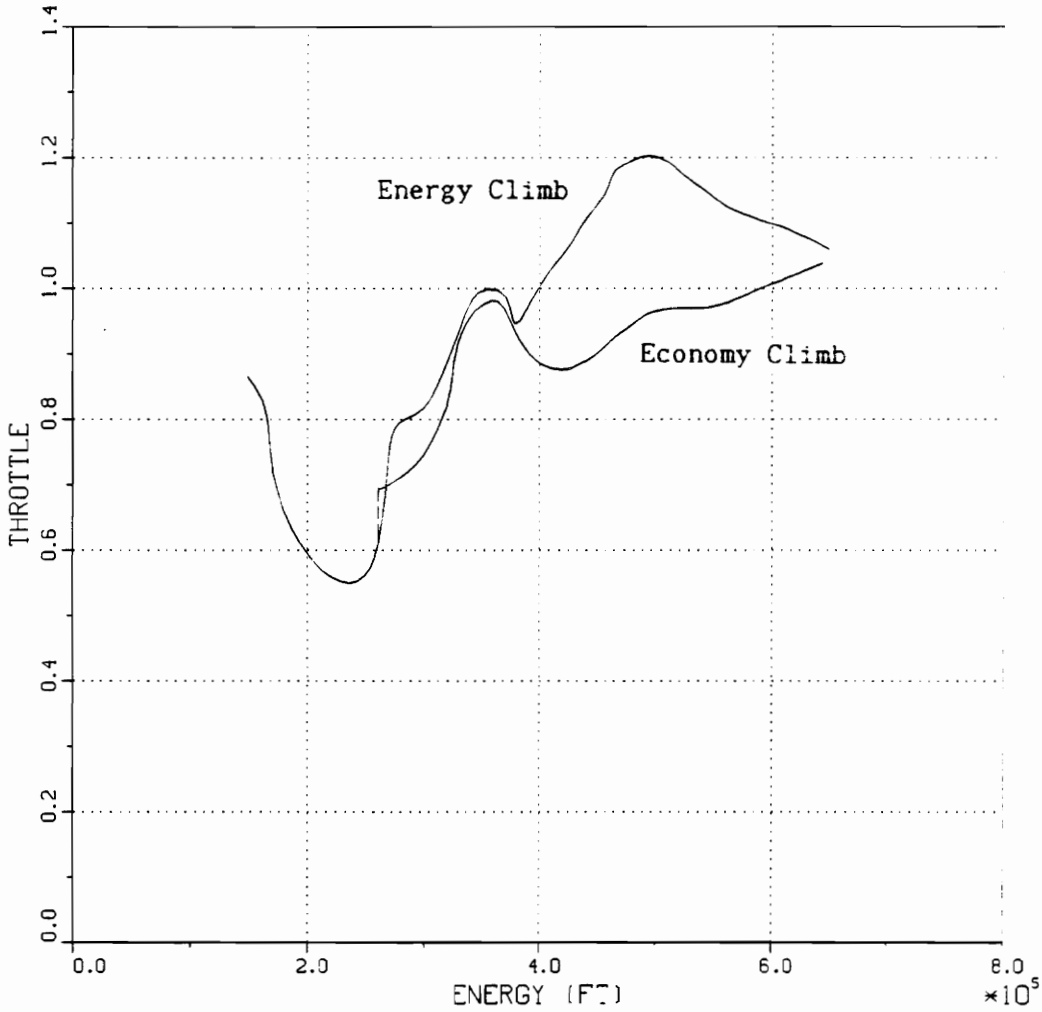

Figure 4-7. Throttle Settings For Energy Rates

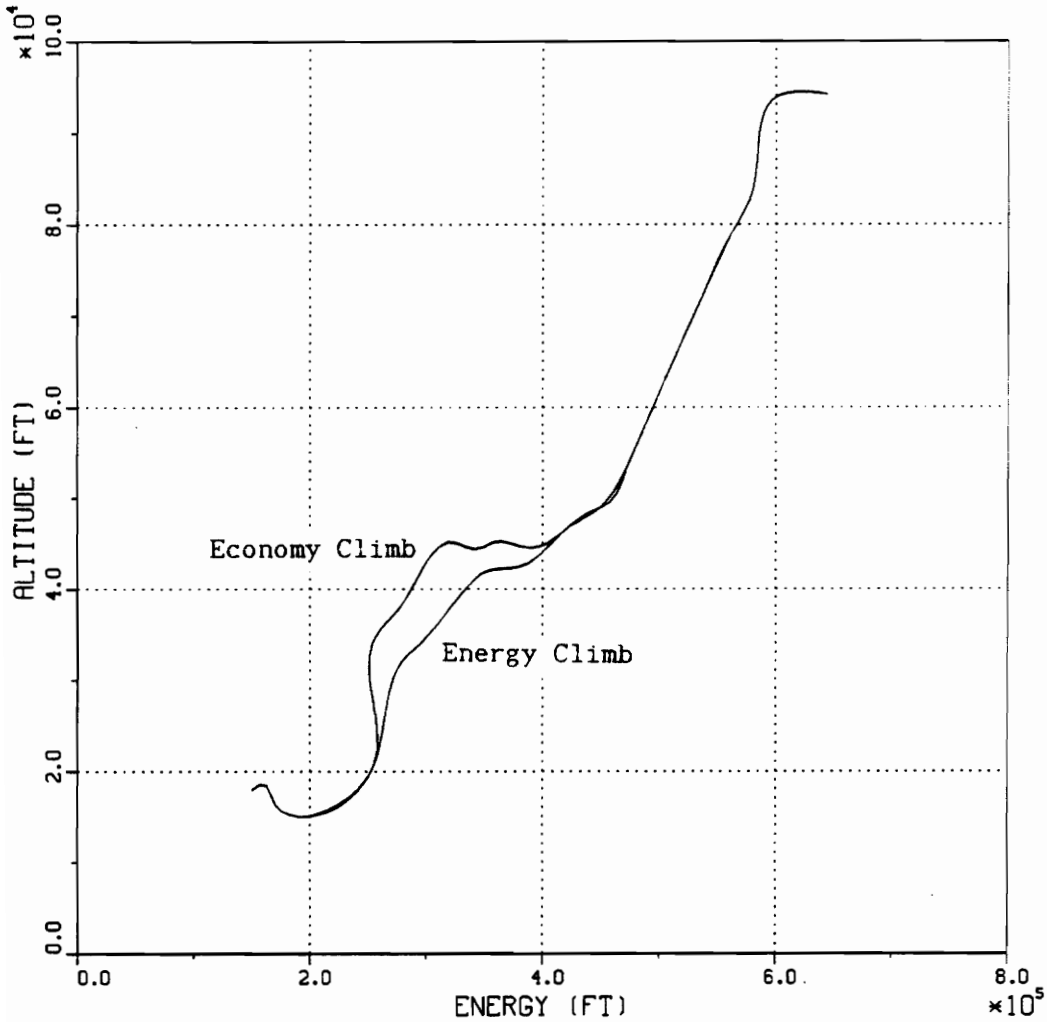

Figure 4-8. Altitudes For Fastest and Economy Climbs

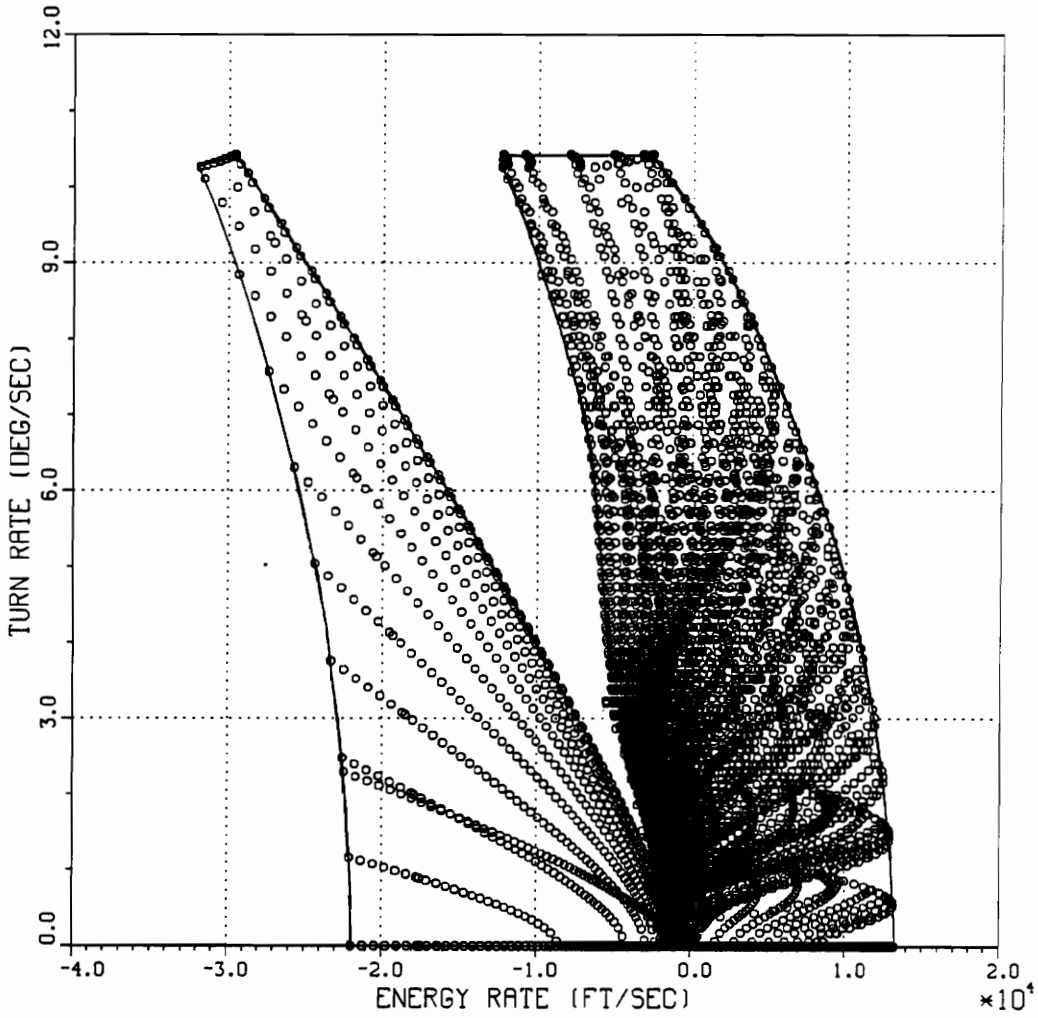

Figure 4-9. Energy-Heading Angle Hodograph, E = 200 kft.

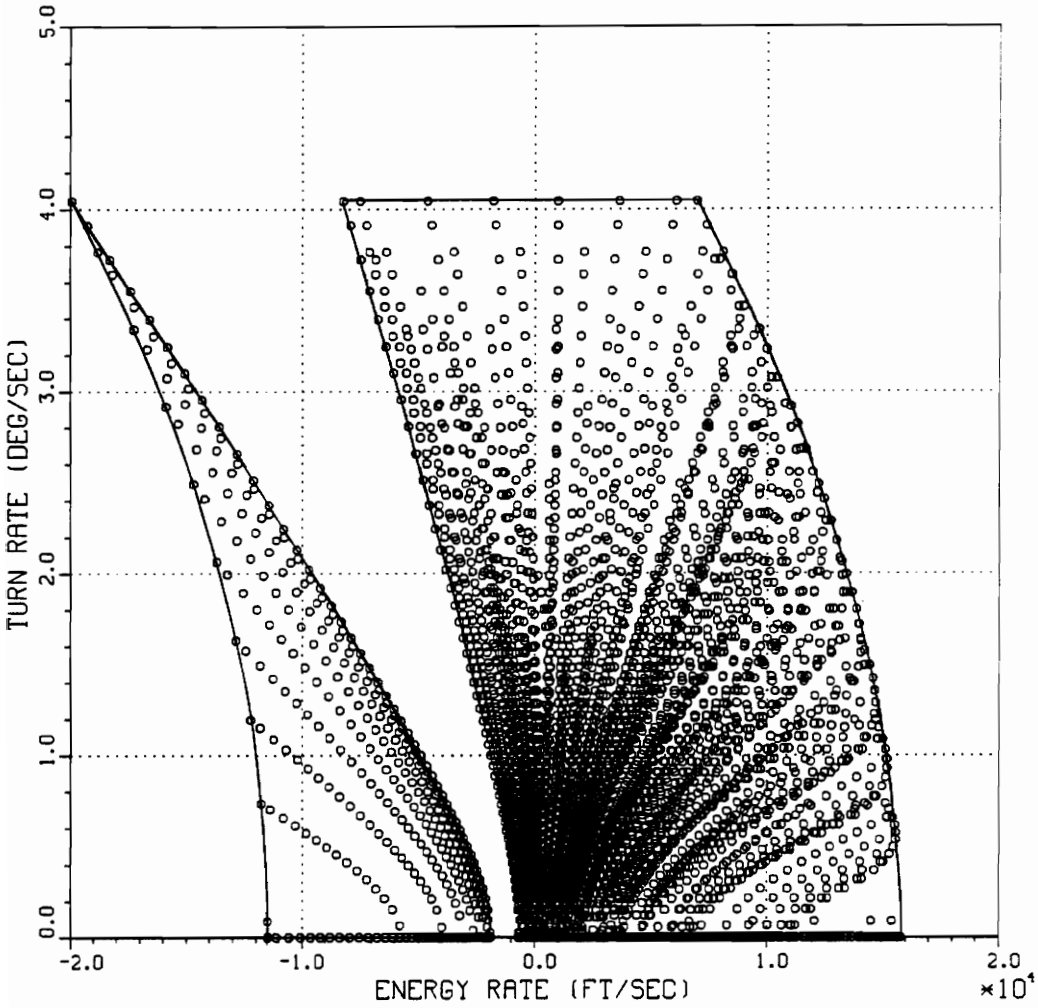

Figure 4-10. Energy-Heading Angle Hodograph, E = 350 kft.

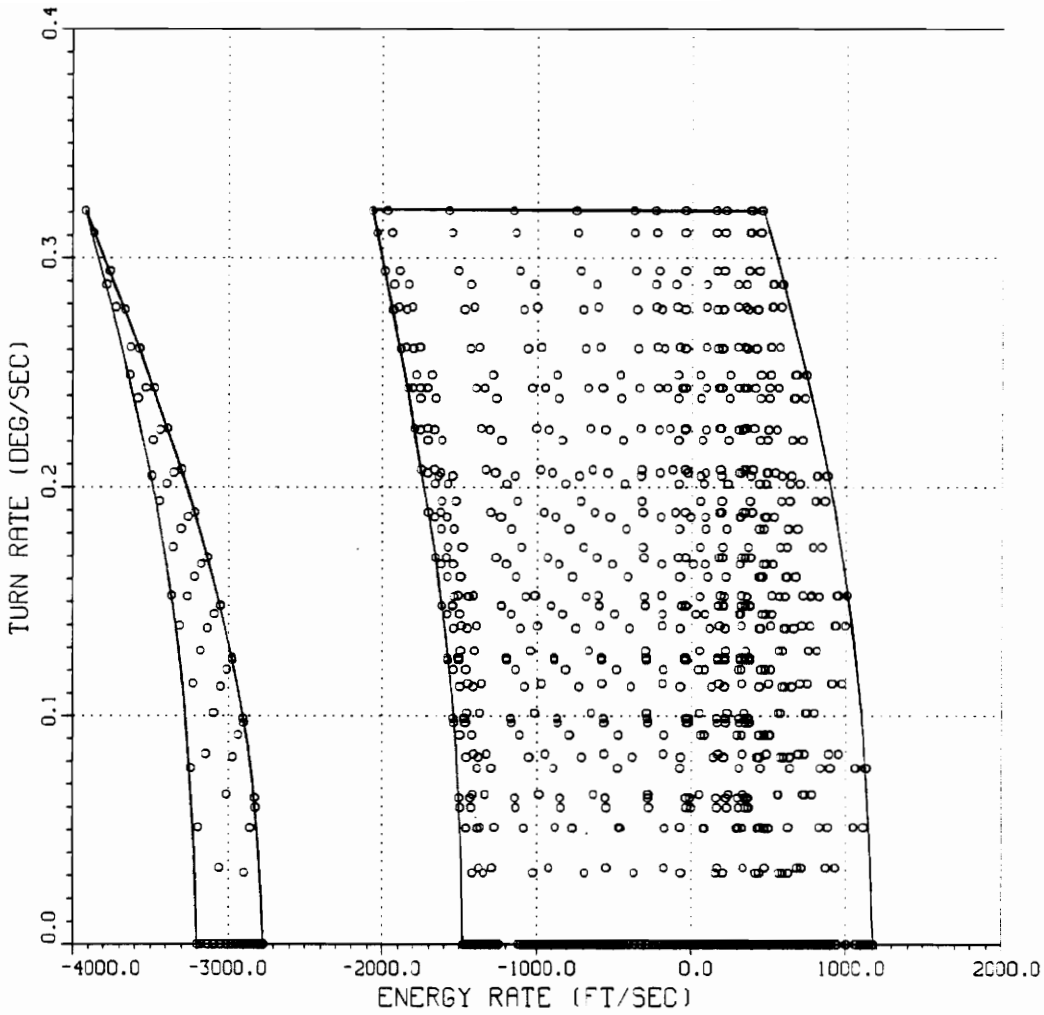

Figure 4-11. Energy-Heading Angle Hodograph, E = 600 kft.

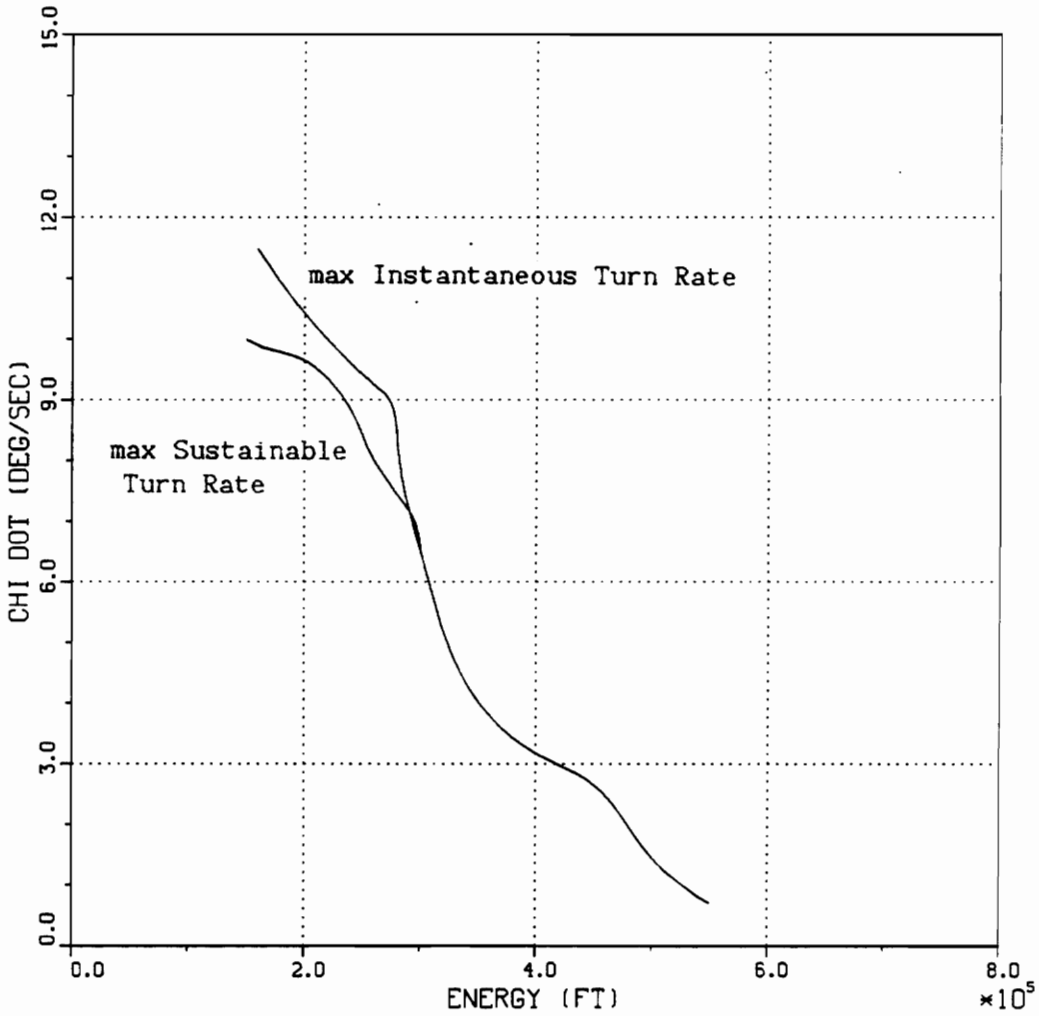

Figure 4-12. Fastest Instantaneous and Fastest Sustainable Turns

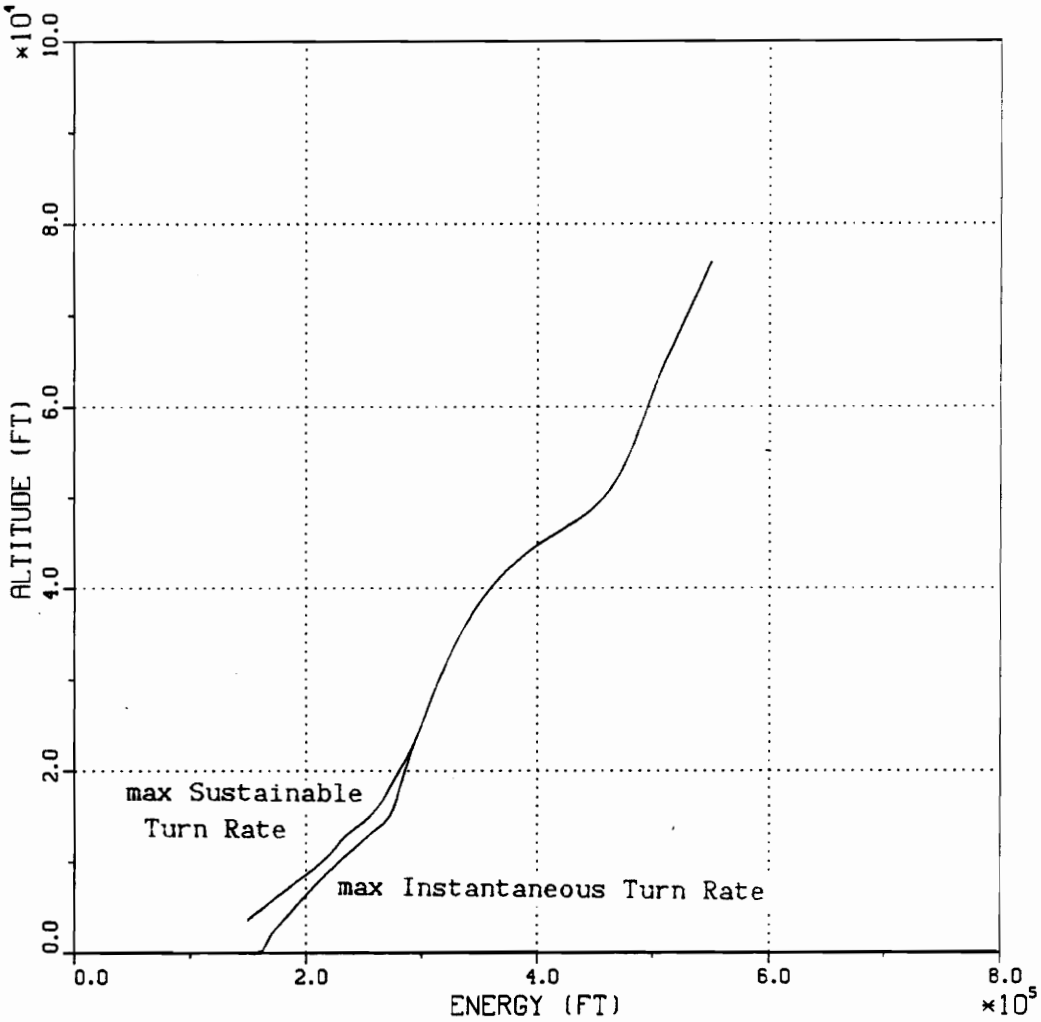

Figure 4-13. Altitudes For Fastest Instantaneous and Fastest Sustainable Turn

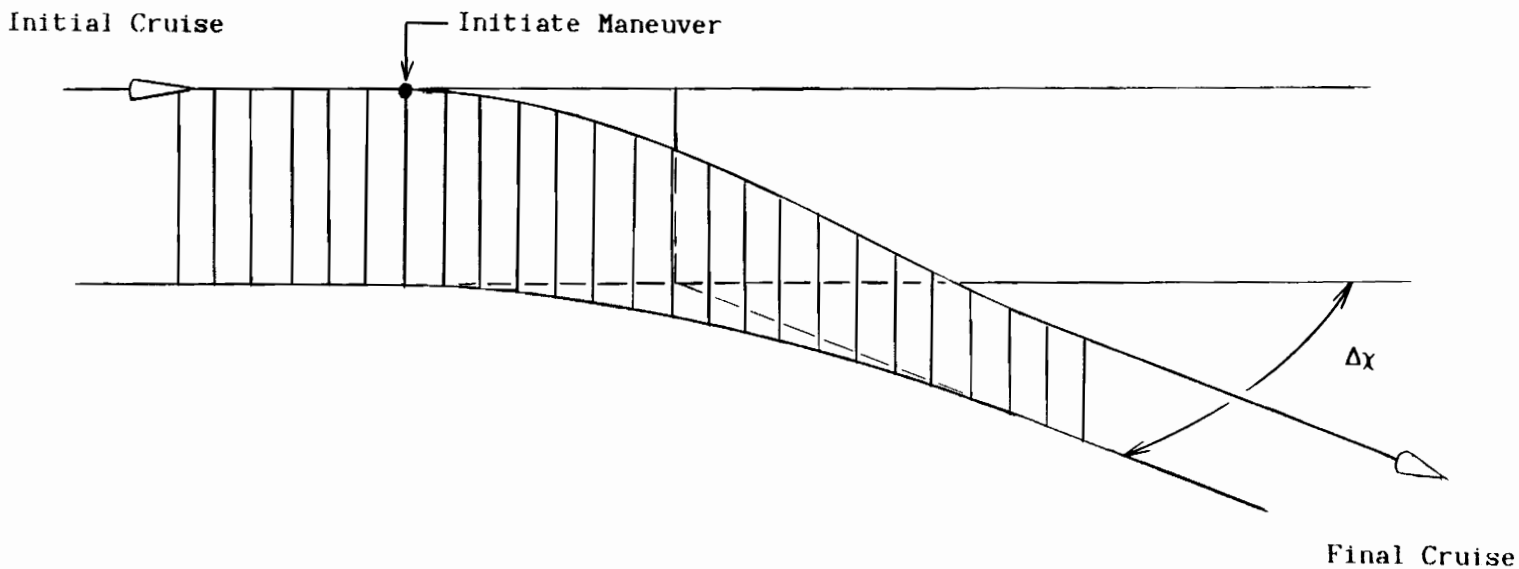

Figure 5-1. Initial transition-to-cruise problem

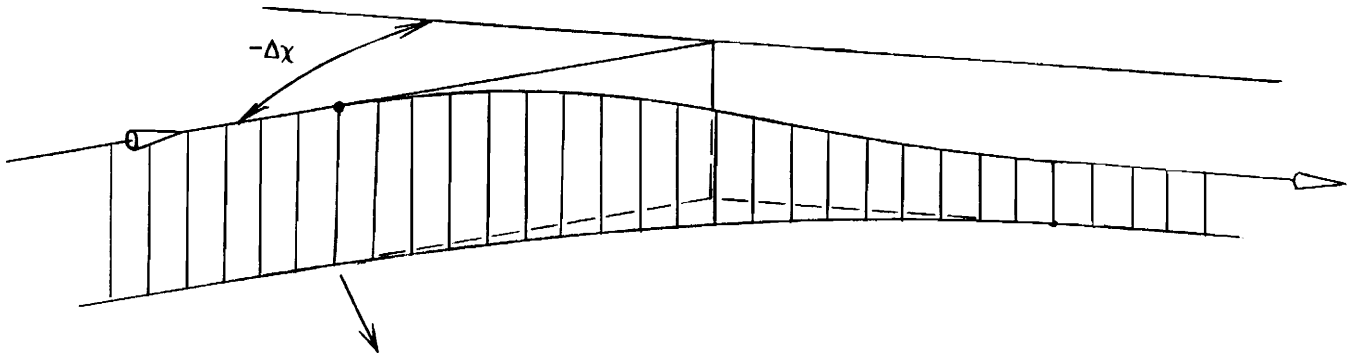

Before Maneuver	Initiate Maneuver(t_0)	Final Cruise
E_{-1}	$E_0 = E_{-1}$	E_f
$\chi_{-1} = 0.$	$\chi_0 = -\Delta\chi$	$\chi_f = 0.$
$\lambda_{E_{-1}}$	$\lambda_{E_0} = ?$	λ_{Ef}
$\lambda_{\chi_{-1}} = 0.$	$\lambda_{\chi_0} = ?$	$\lambda_{\chi f} = 0.$
$\bar{\lambda}_{x_{-1}}$	$\bar{\lambda}_{x_0} = \bar{\lambda}_{xf}$	$\bar{\lambda}_{xf}$
$\bar{\lambda}_{y_{-1}} = 0.$	$\bar{\lambda}_{y_0} = \bar{\lambda}_{yf}$	$\bar{\lambda}_{yf} = 0.$
$\bar{\lambda}_{F_{-1}}$	$\bar{\lambda}_{F_0} = \bar{\lambda}_{Ff}$	$\bar{\lambda}_{Ff}$

Figure 5-2. Transition-to-cruise problem restated

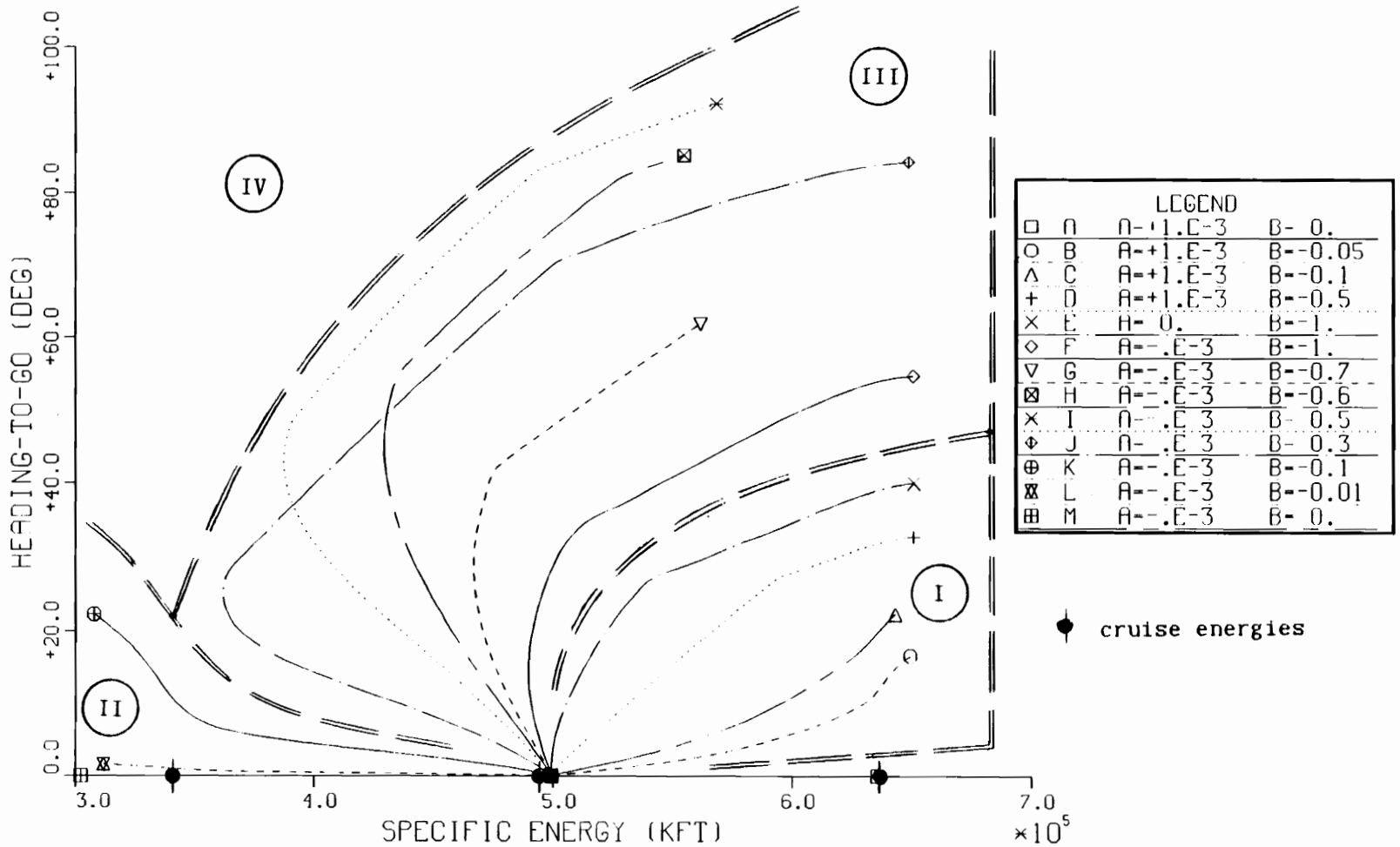

Figure 5-3. Transition to cruise: Heading vs. Specific Energy

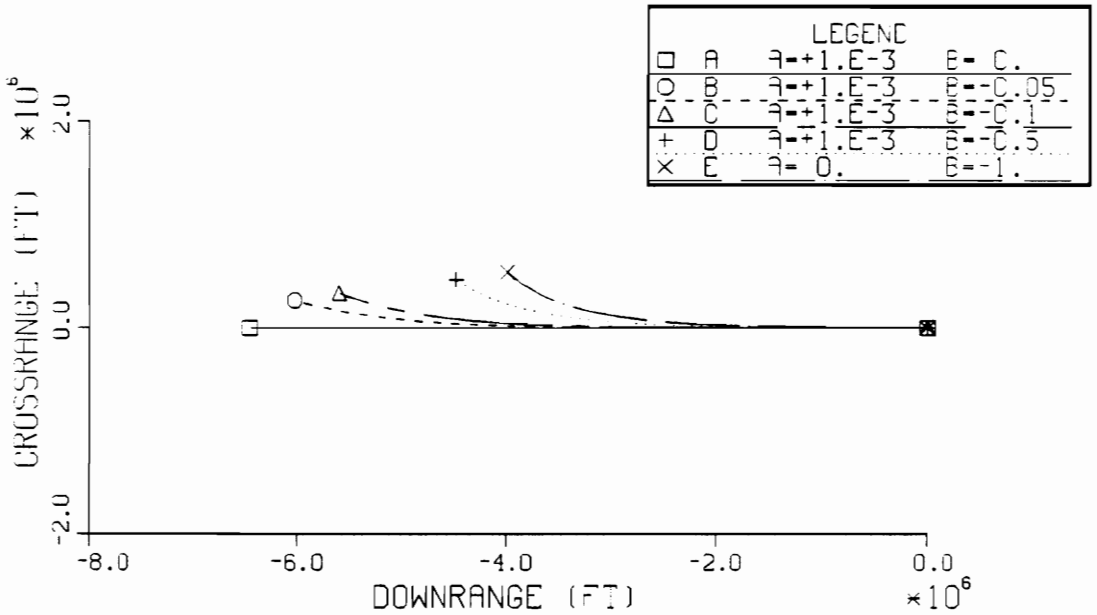

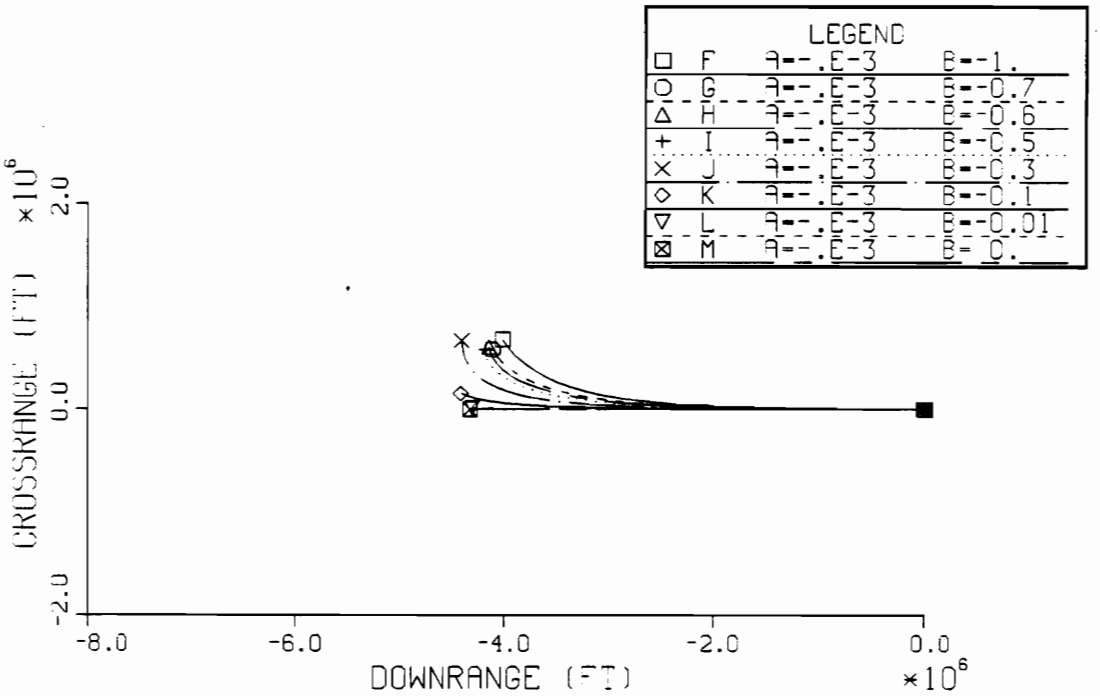

Figure 5-4. Transition to cruise: Ground Track

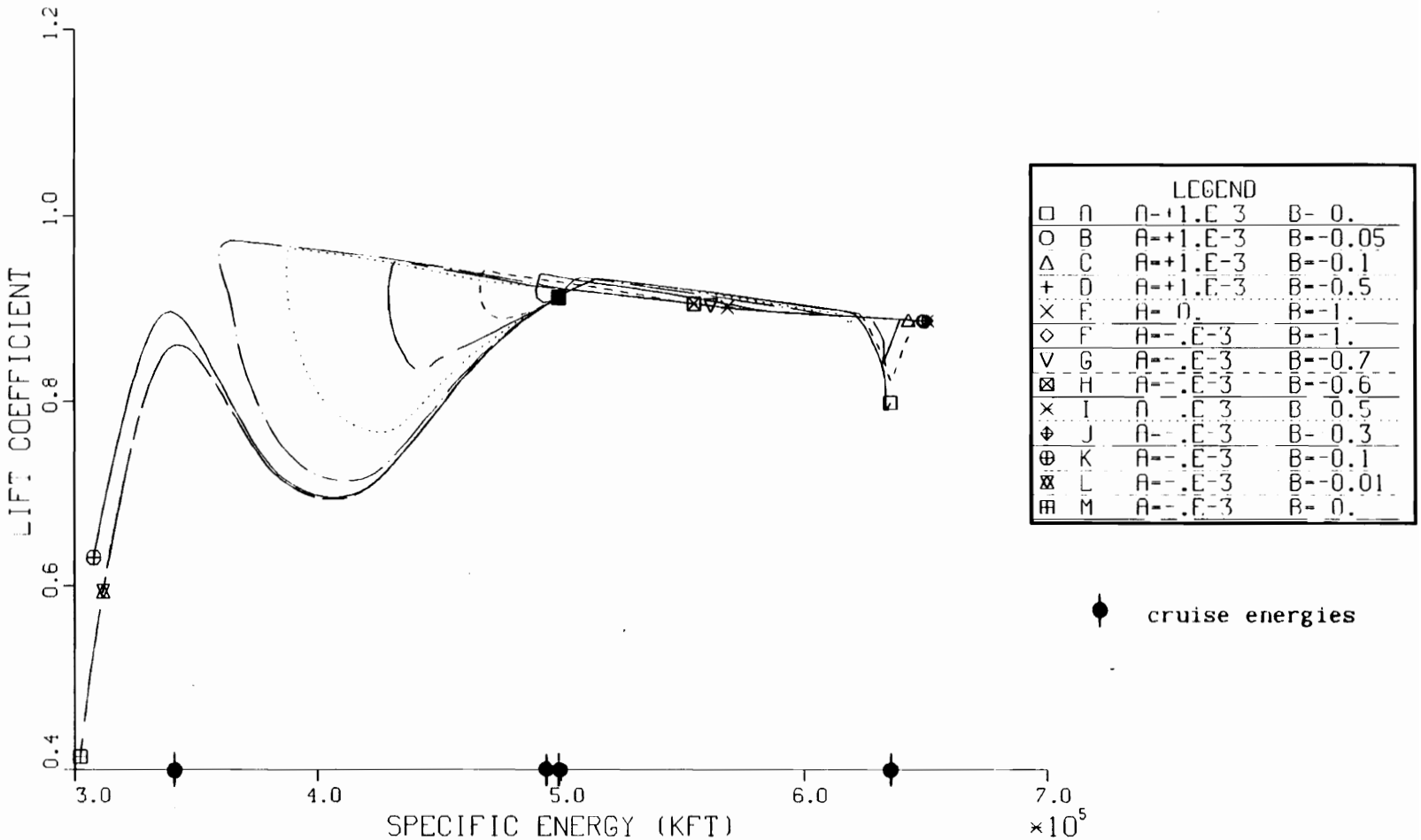

Figure 5-5. Transition to cruise: Lift Coefficient vs. Specific Energy

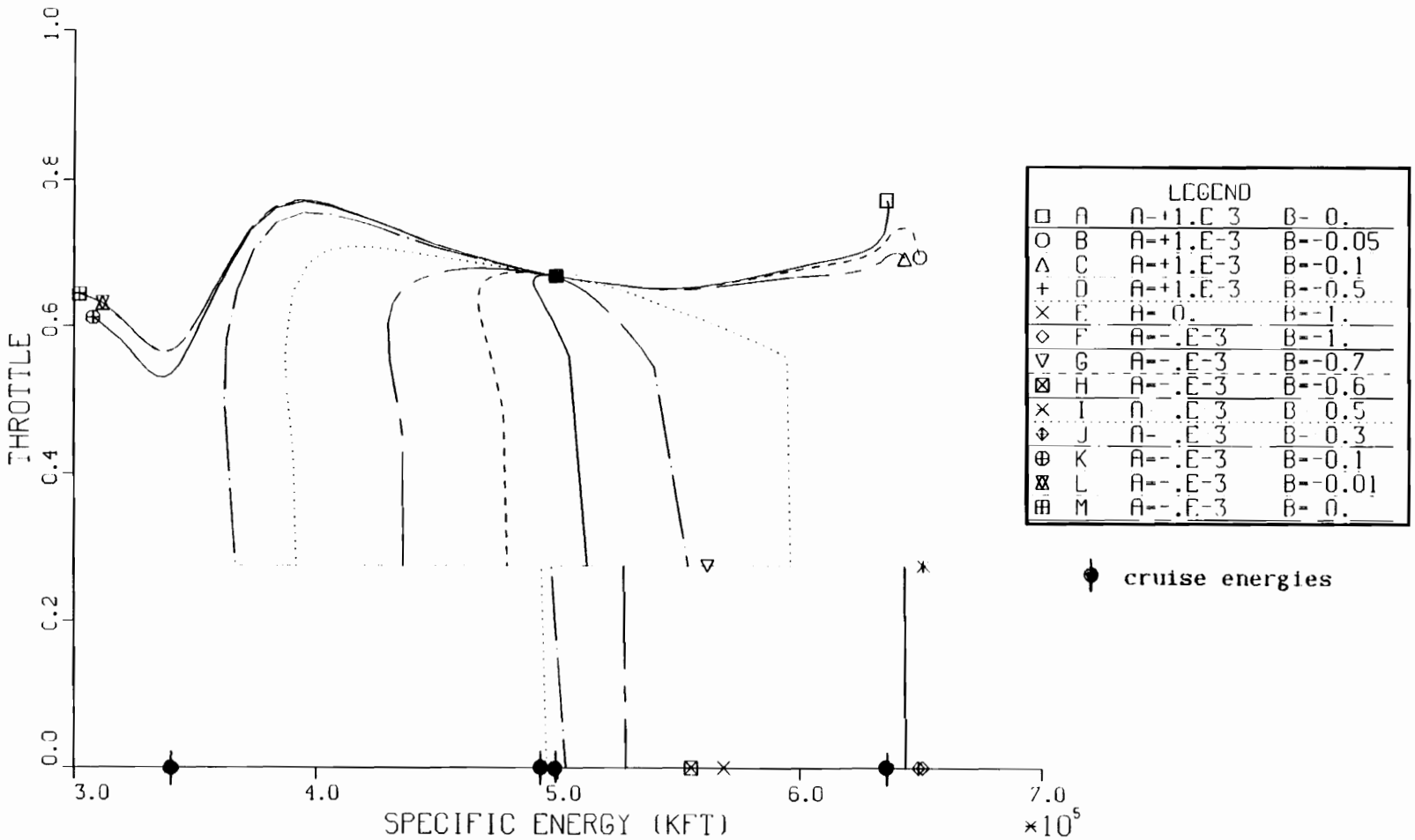

Figure 5-6. Transition to cruise: Throttle vs. Specific Energy

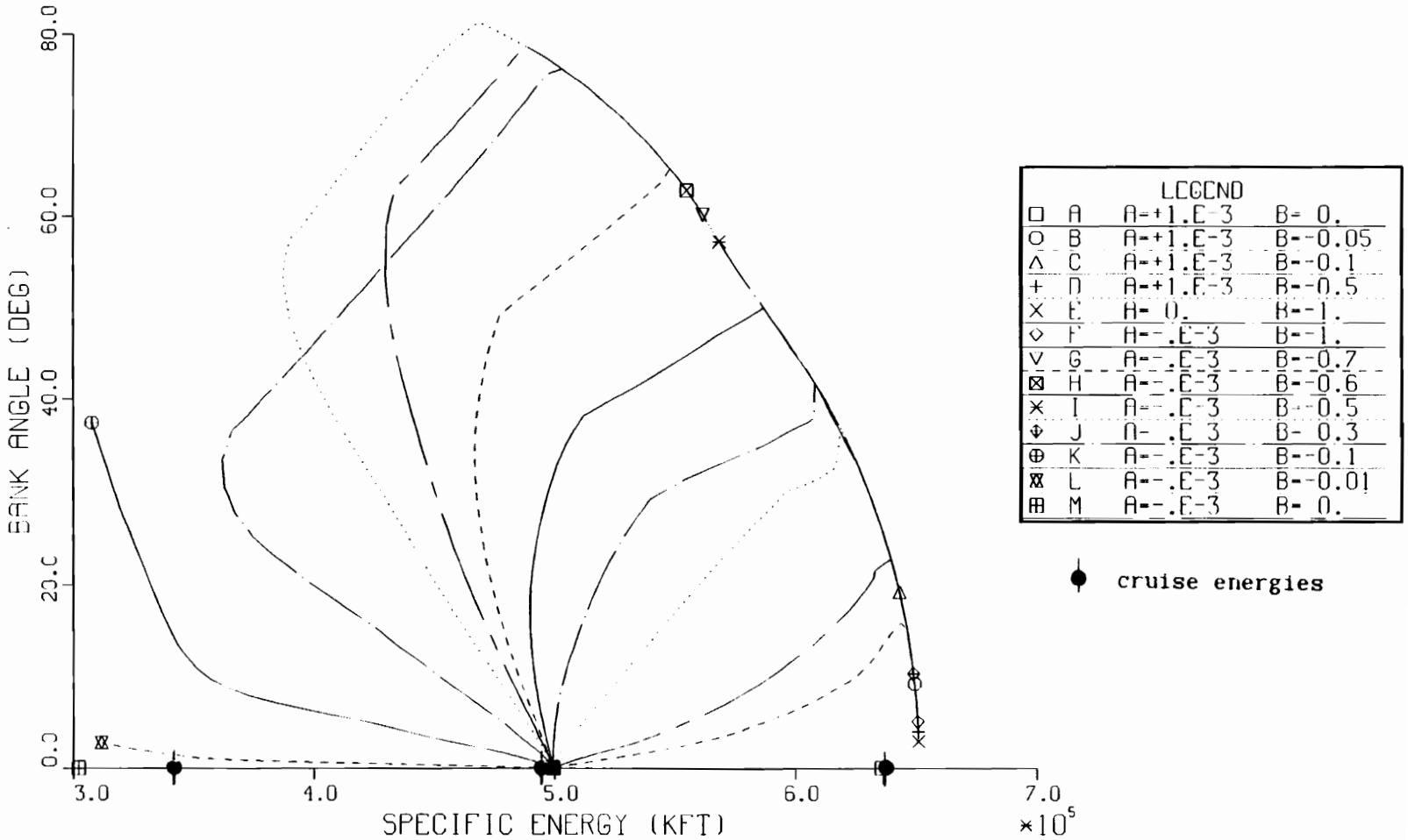

Figure 5-7. Transition to cruise: Bank Angle vs. Specific Energy

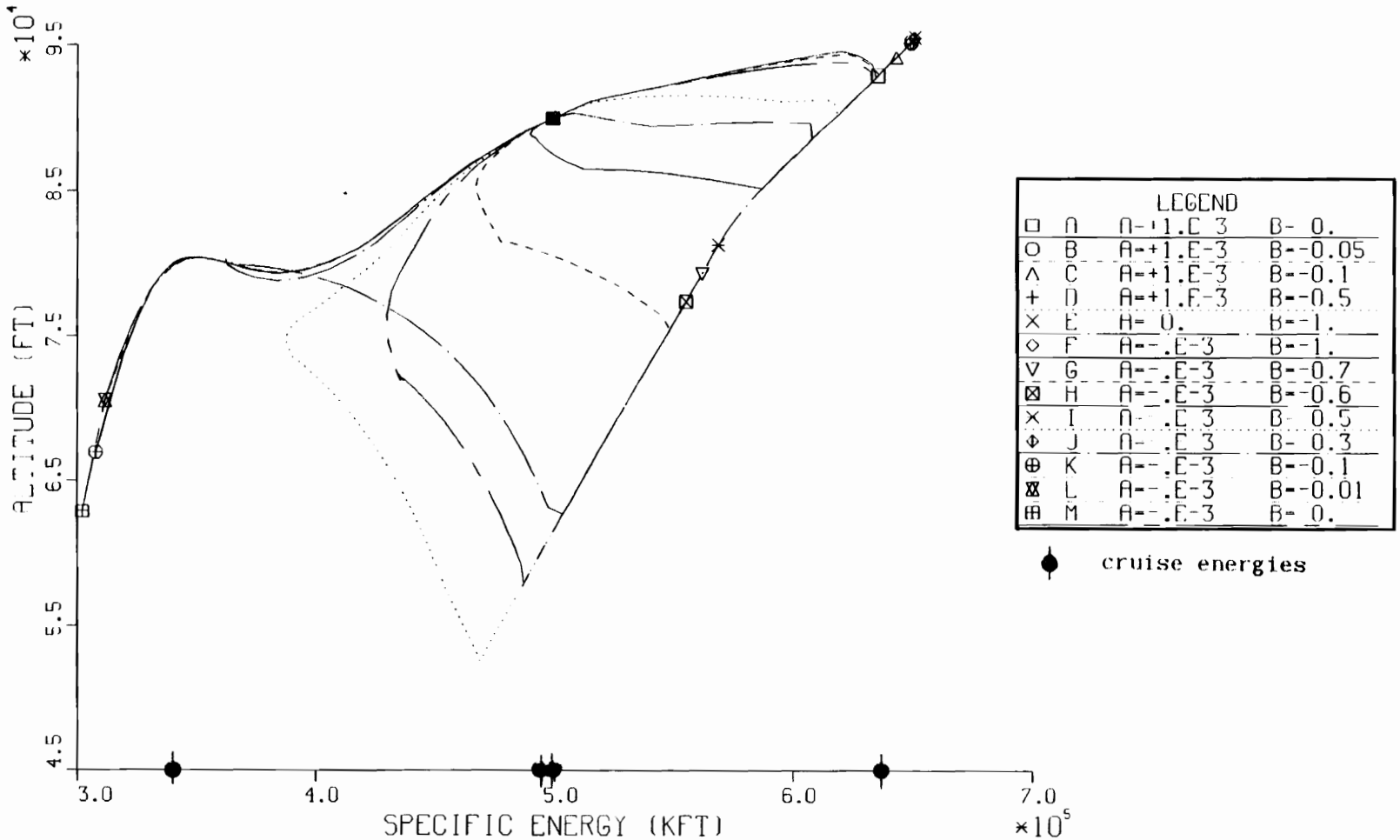

Figure 5-8. Transition to cruise: Altitude vs. Specific Energy

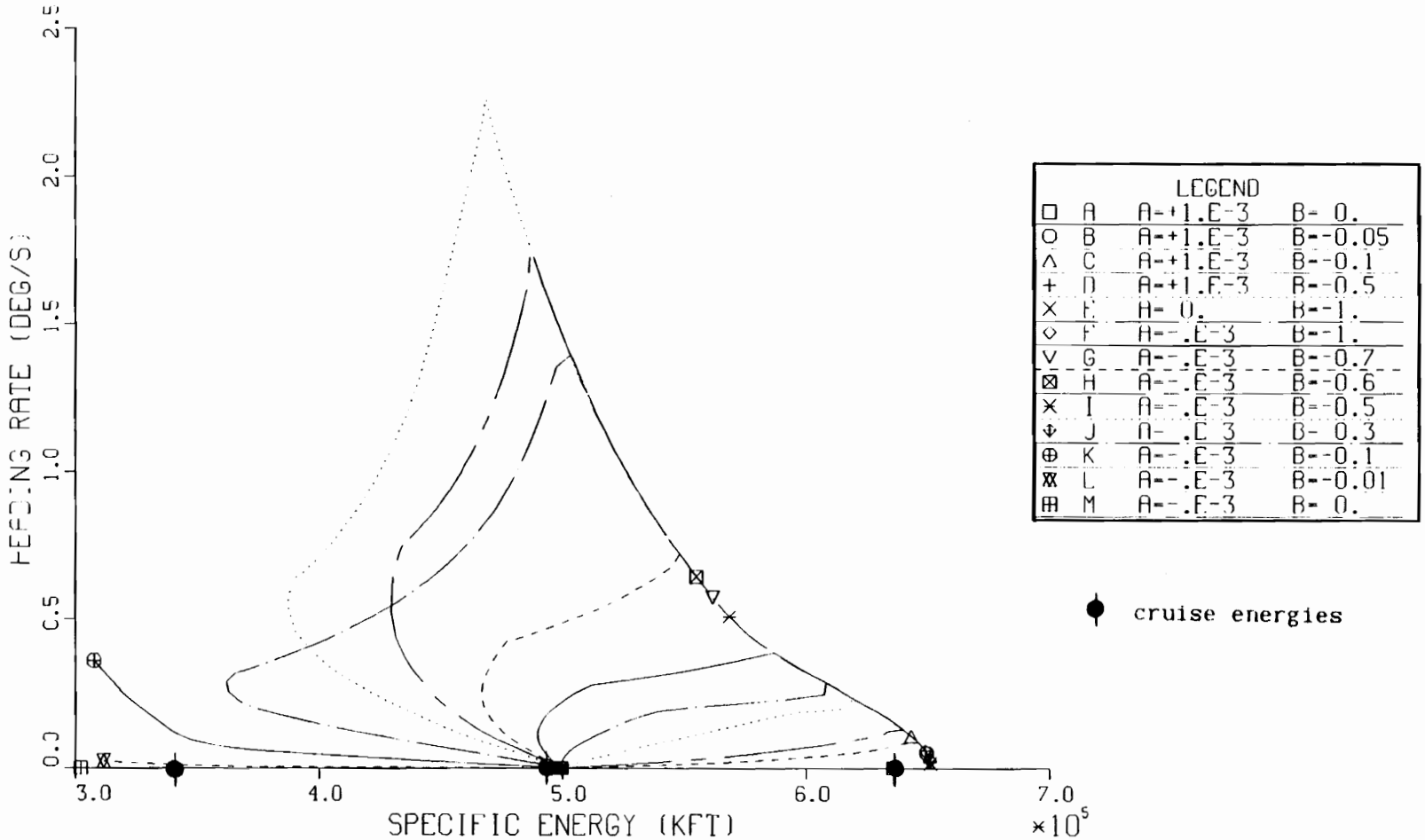

Figure 5-9. Transition to cruise: Heading Rate vs. Specific Energy

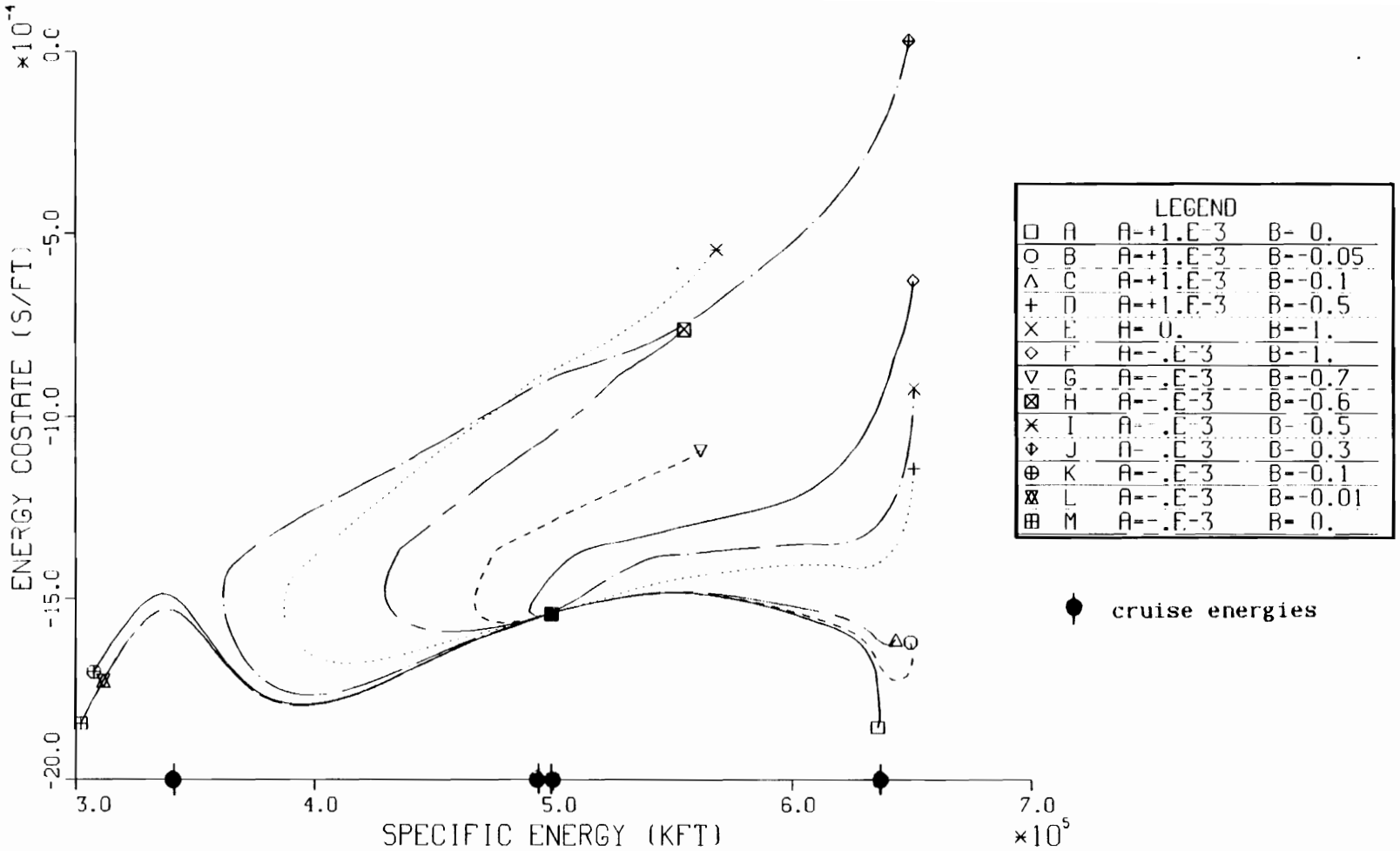

Figure 5-10. Transition to cruise: Energy Costate vs. Specific Energy

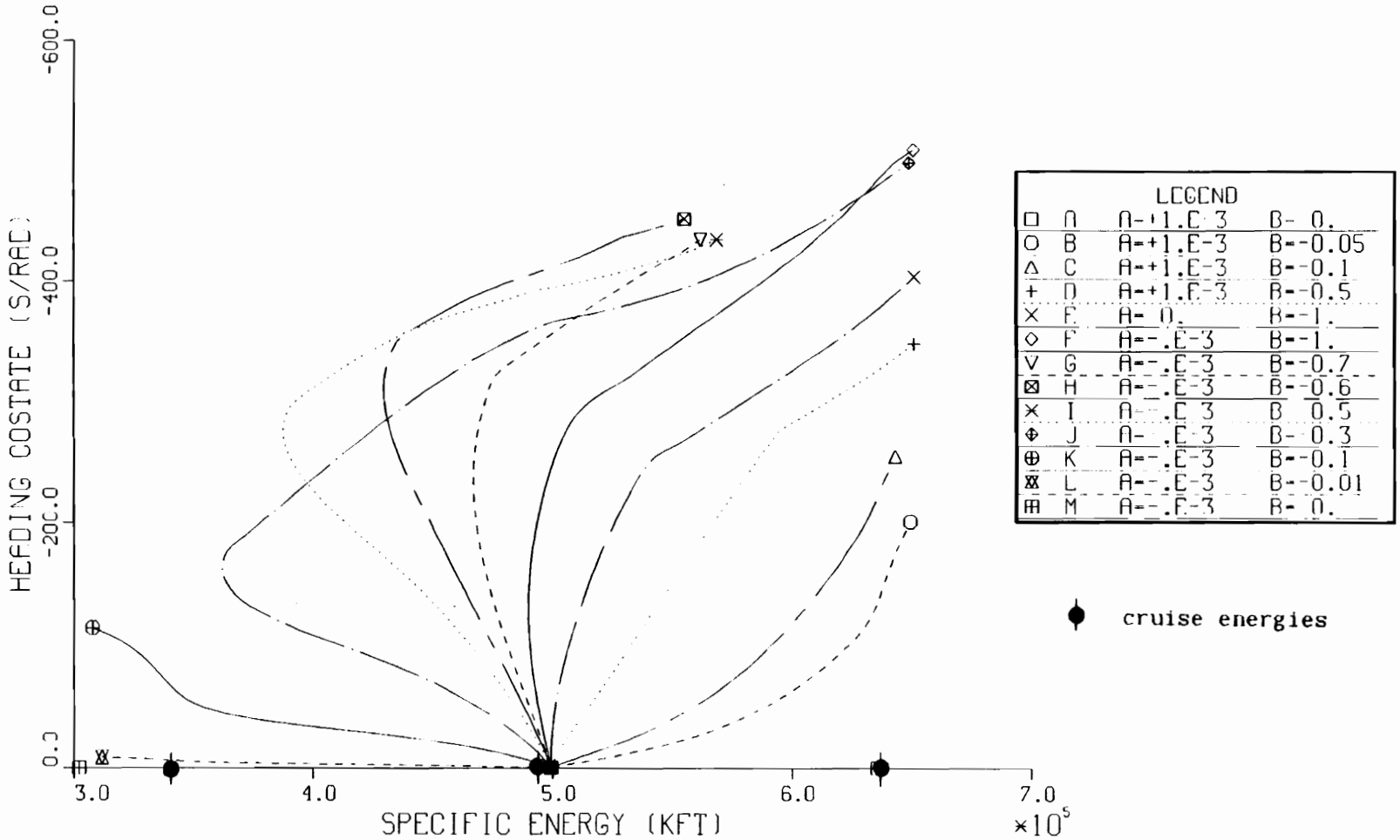

Figure 5-11. Transition to cruise: Heading Costate vs. Specific Energy

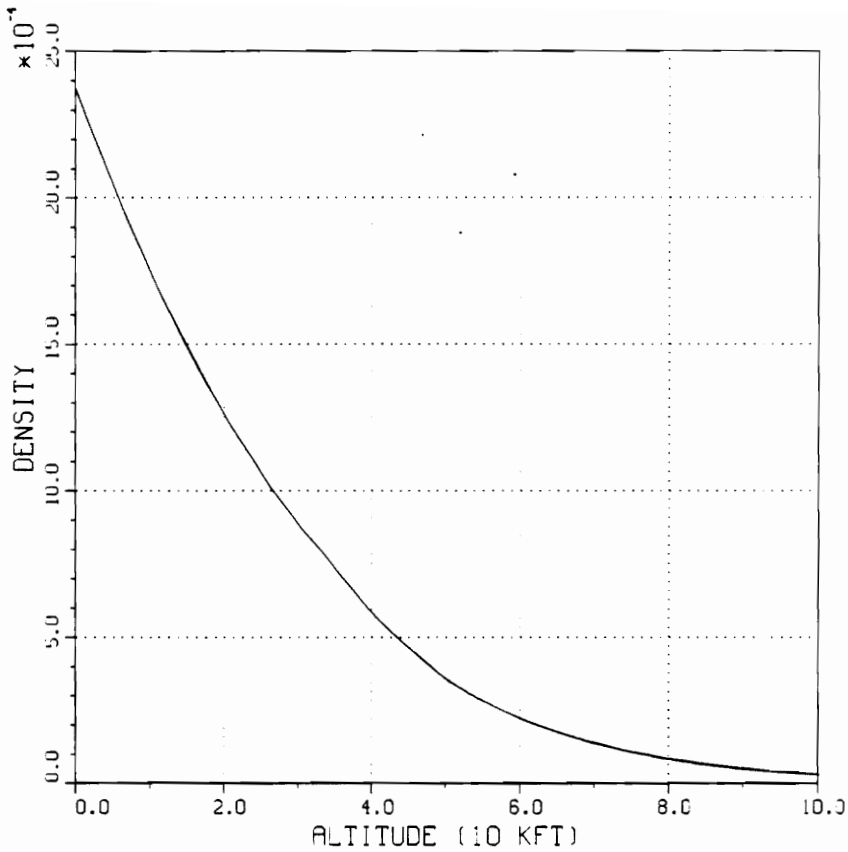

Figure A-1. Air Density

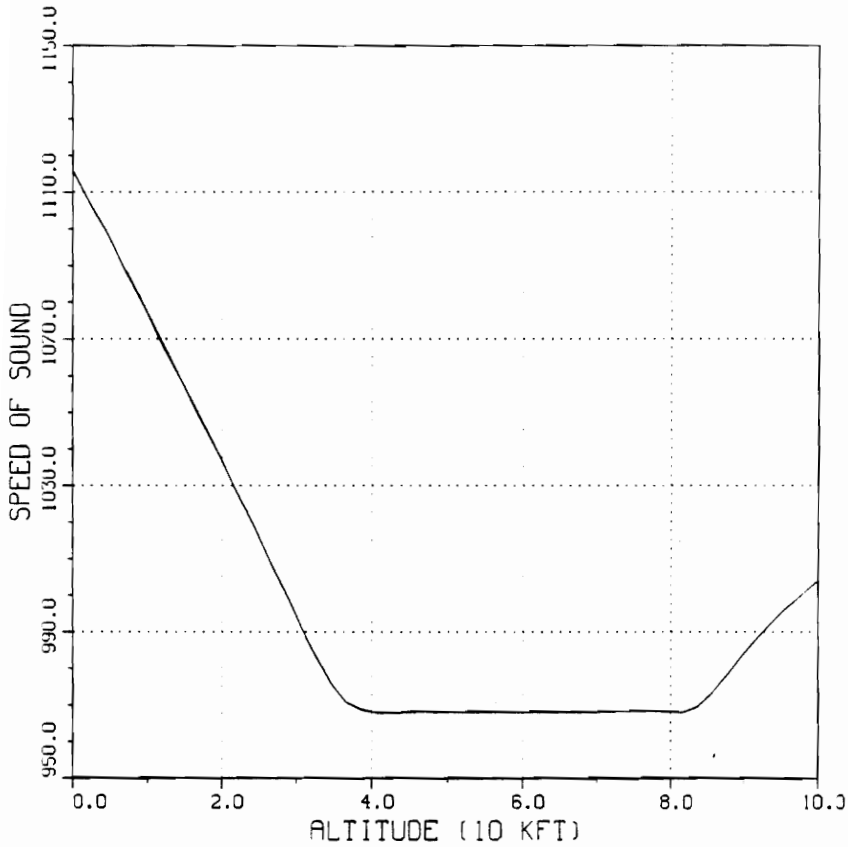

Figure A-2. Sonic Speed

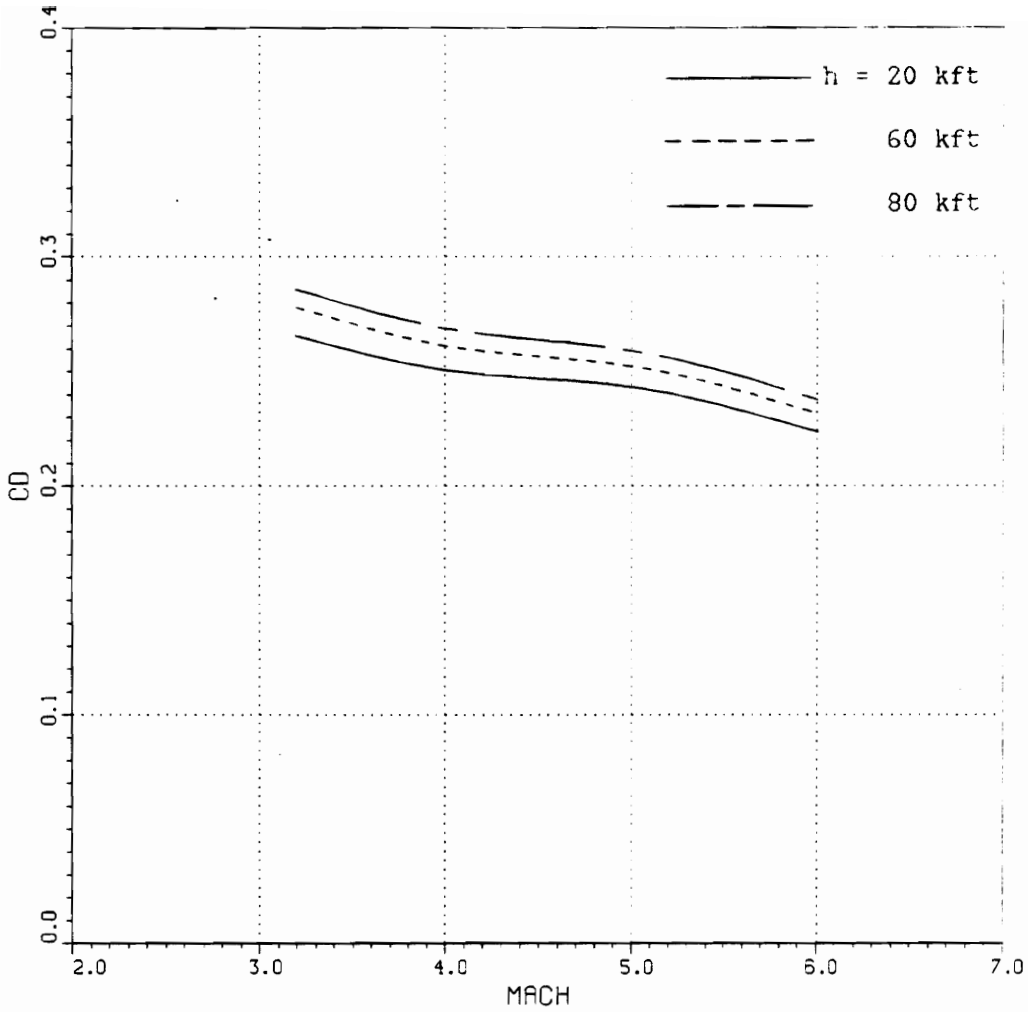

Figure A-3. Drag Coefficient vs. Mach:

C_L = 0.8, h varying

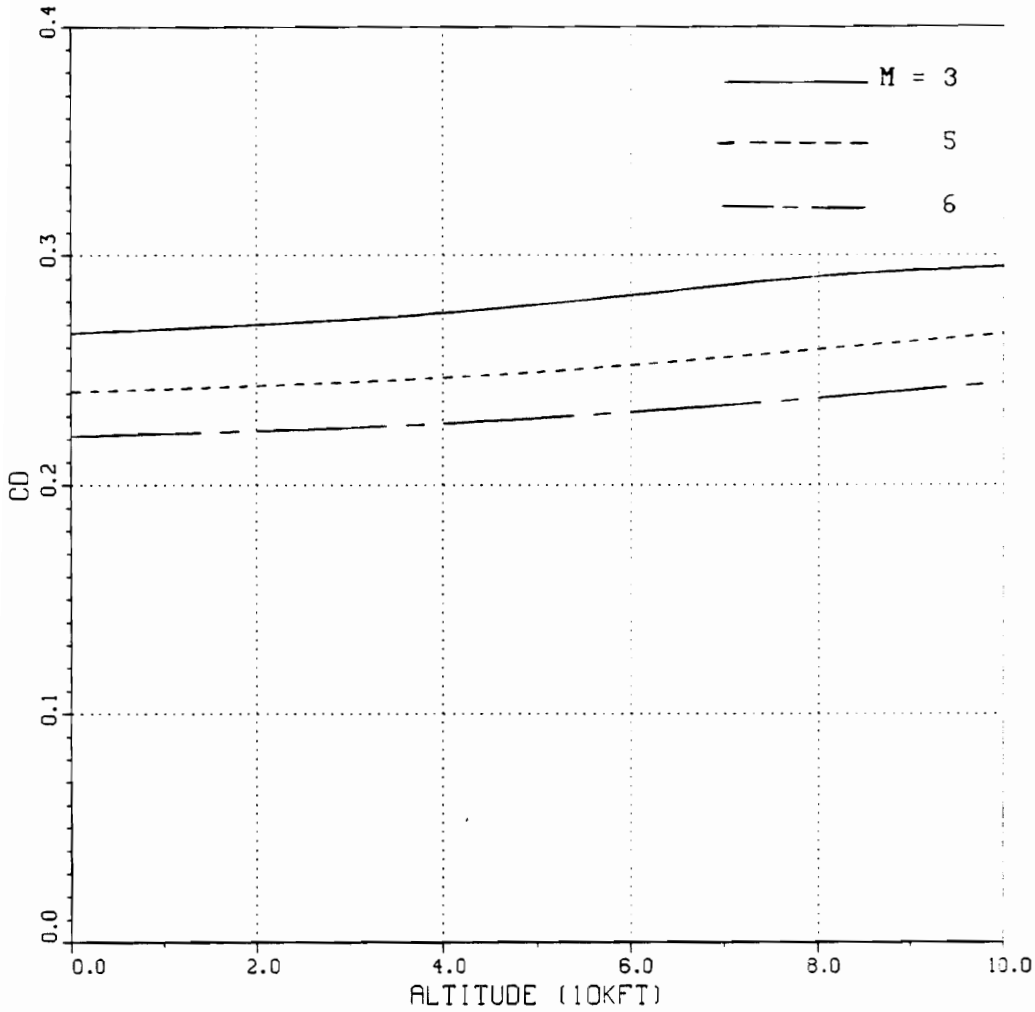

Figure A-4. Drag Coefficient vs. Altitude:

C_L = 0.8, M varying

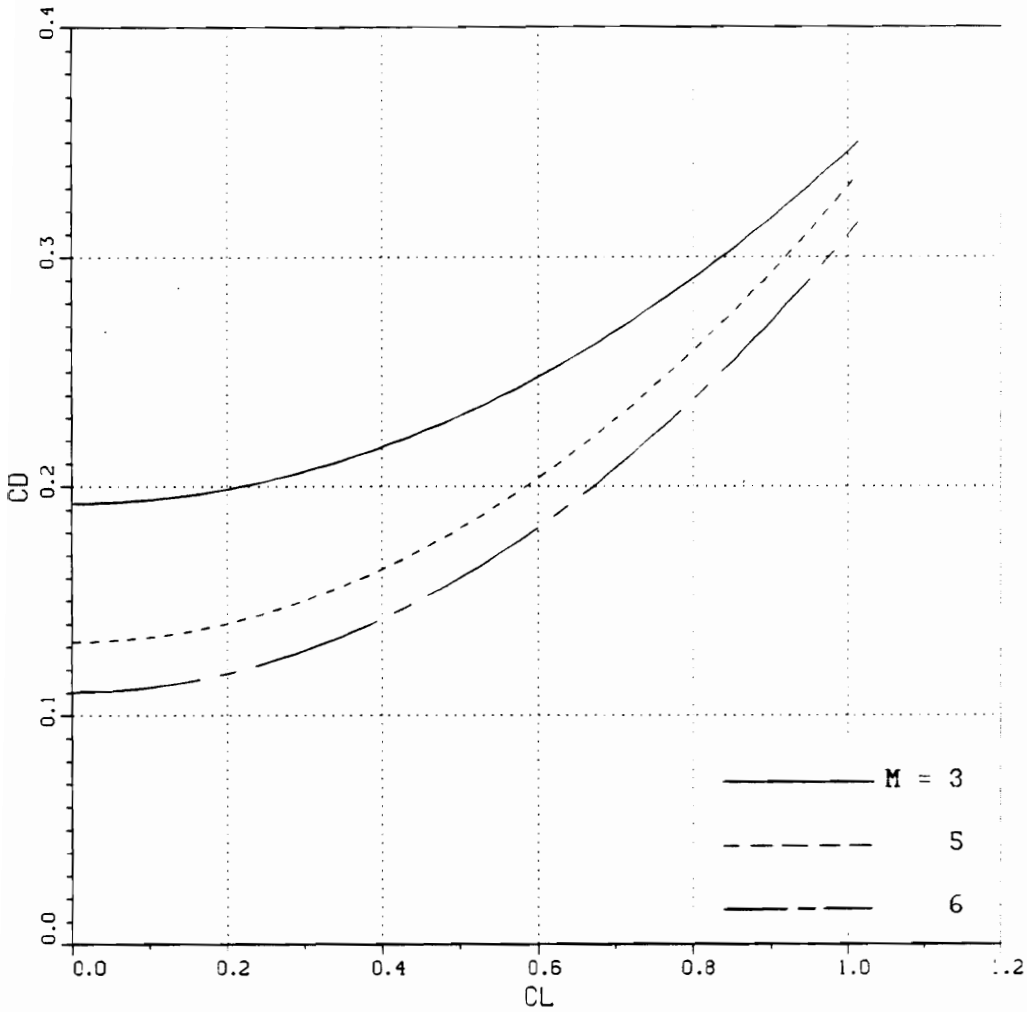

Figure A-5. Drag Coefficient vs. Lift Coefficient:

h = 80 kft, M varying

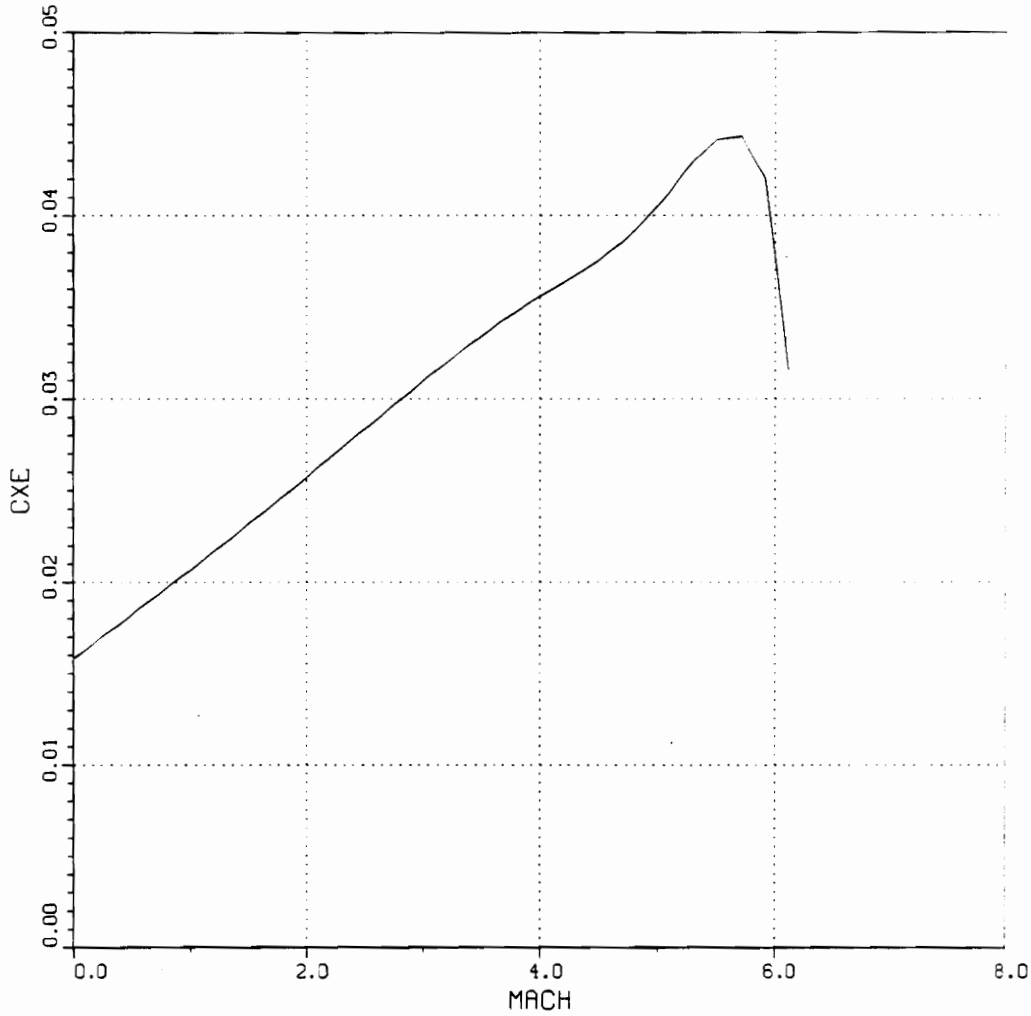

Figure A-6. Inlet Drag Coefficient vs. Mach

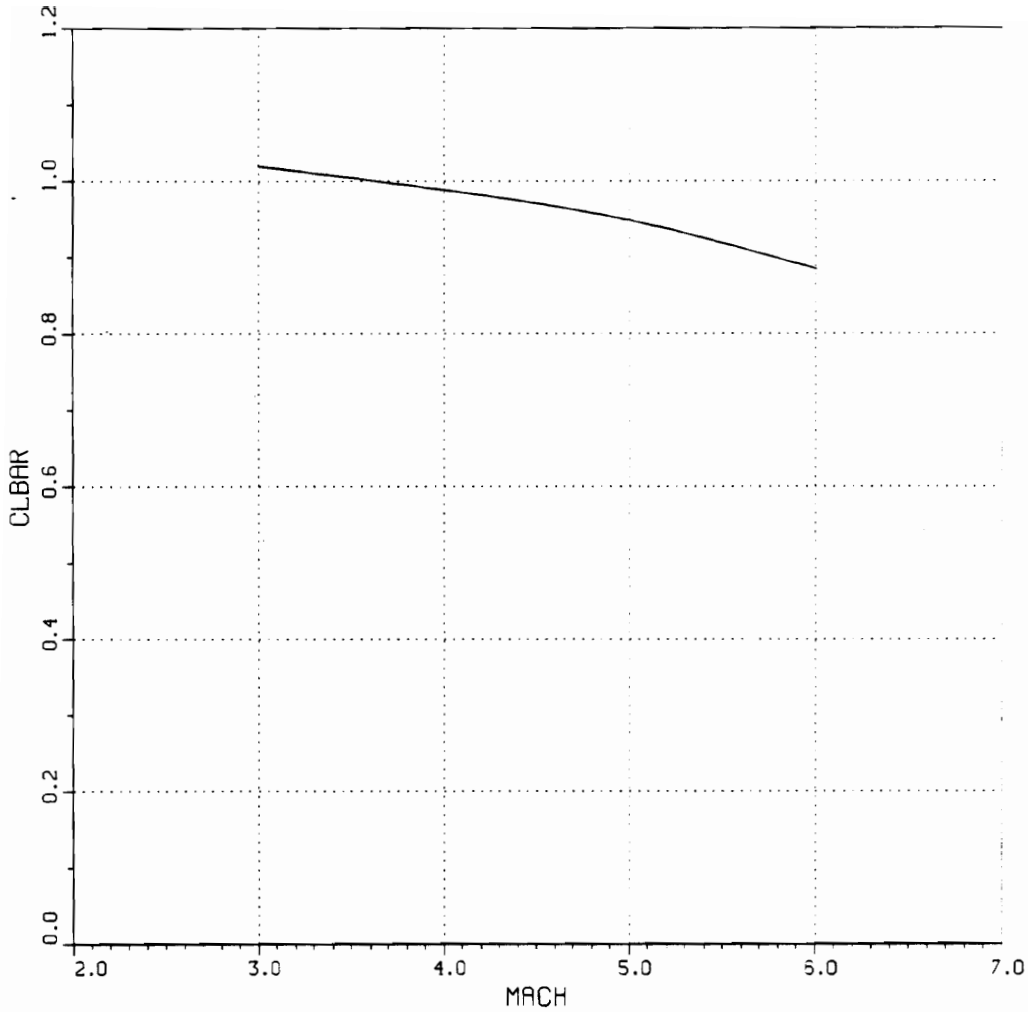

Figure A-7. Maximum Lift Coefficient vs. Mach

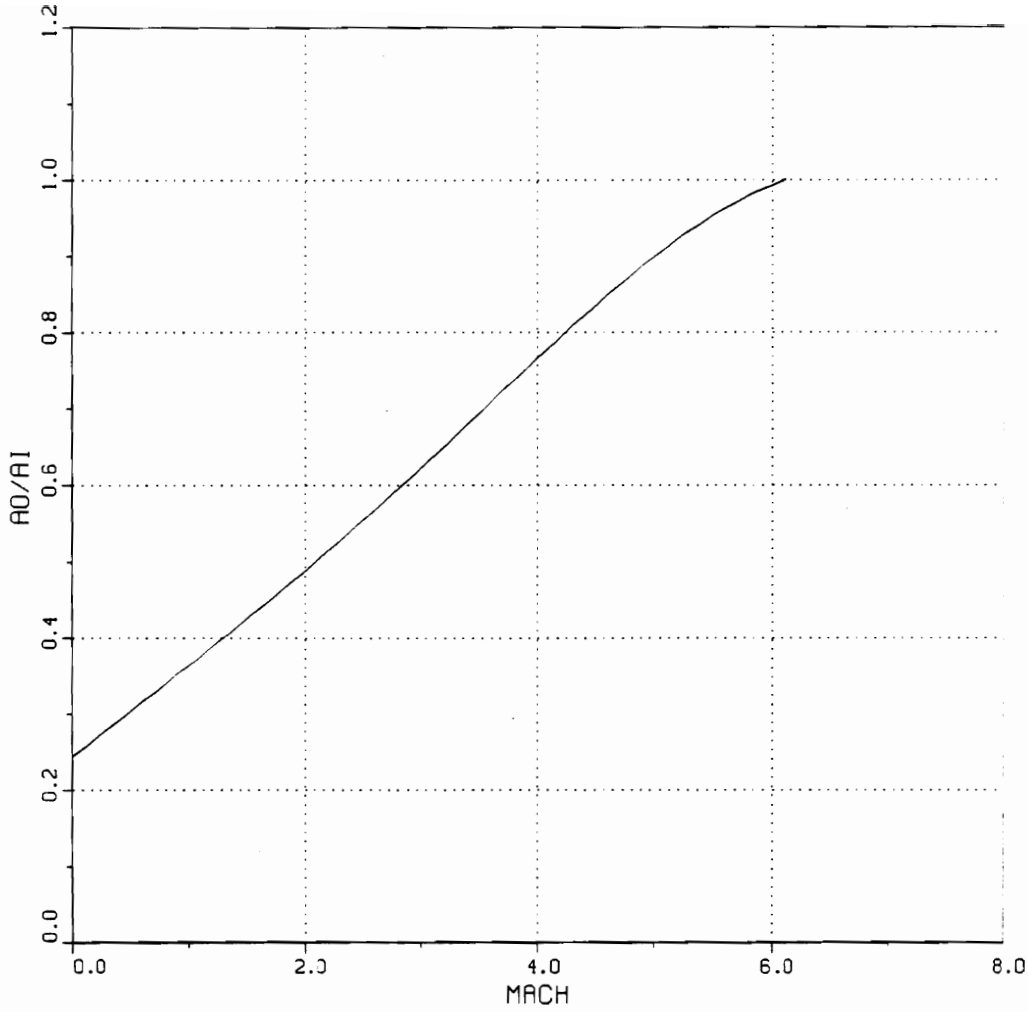

Figure A-8. Engine Capture Ratio vs. Mach

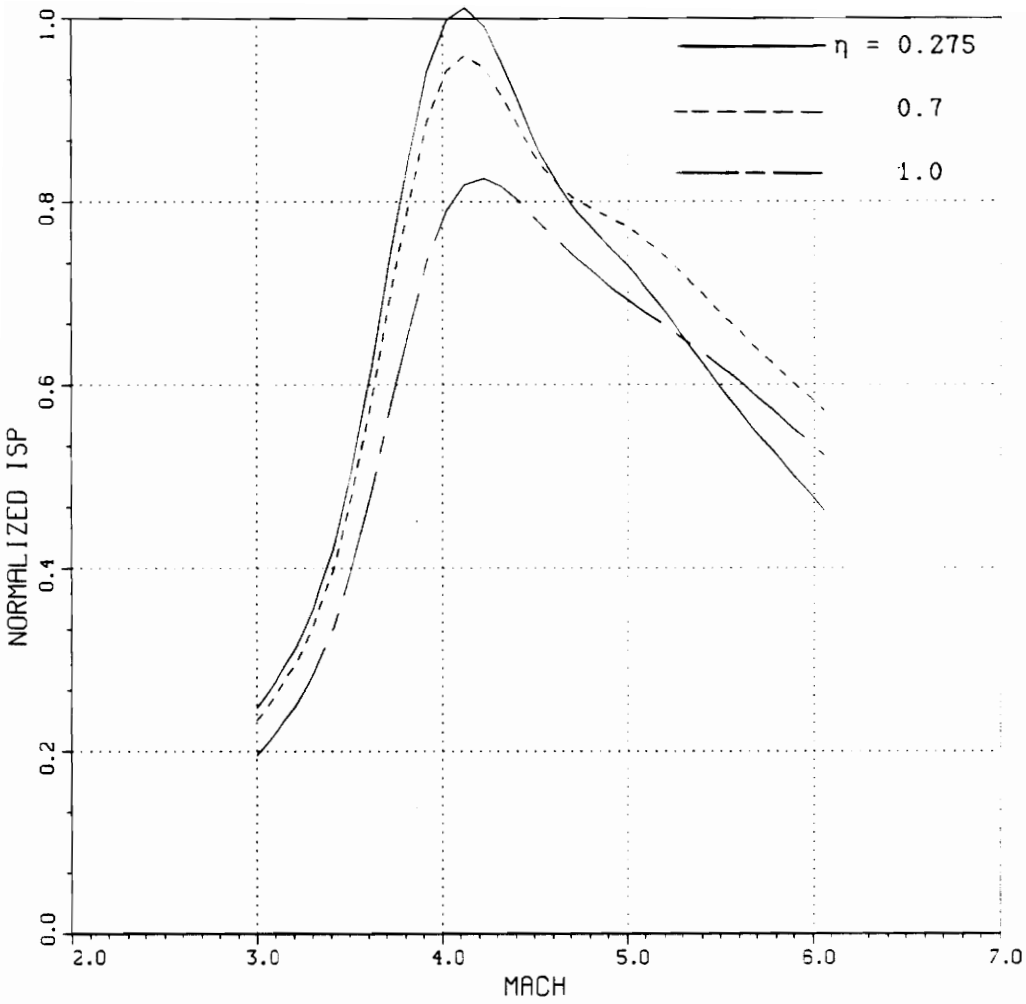

Figure A-9. Thrust Specific Impulse vs. Mach:

h = 80 kft, η varying

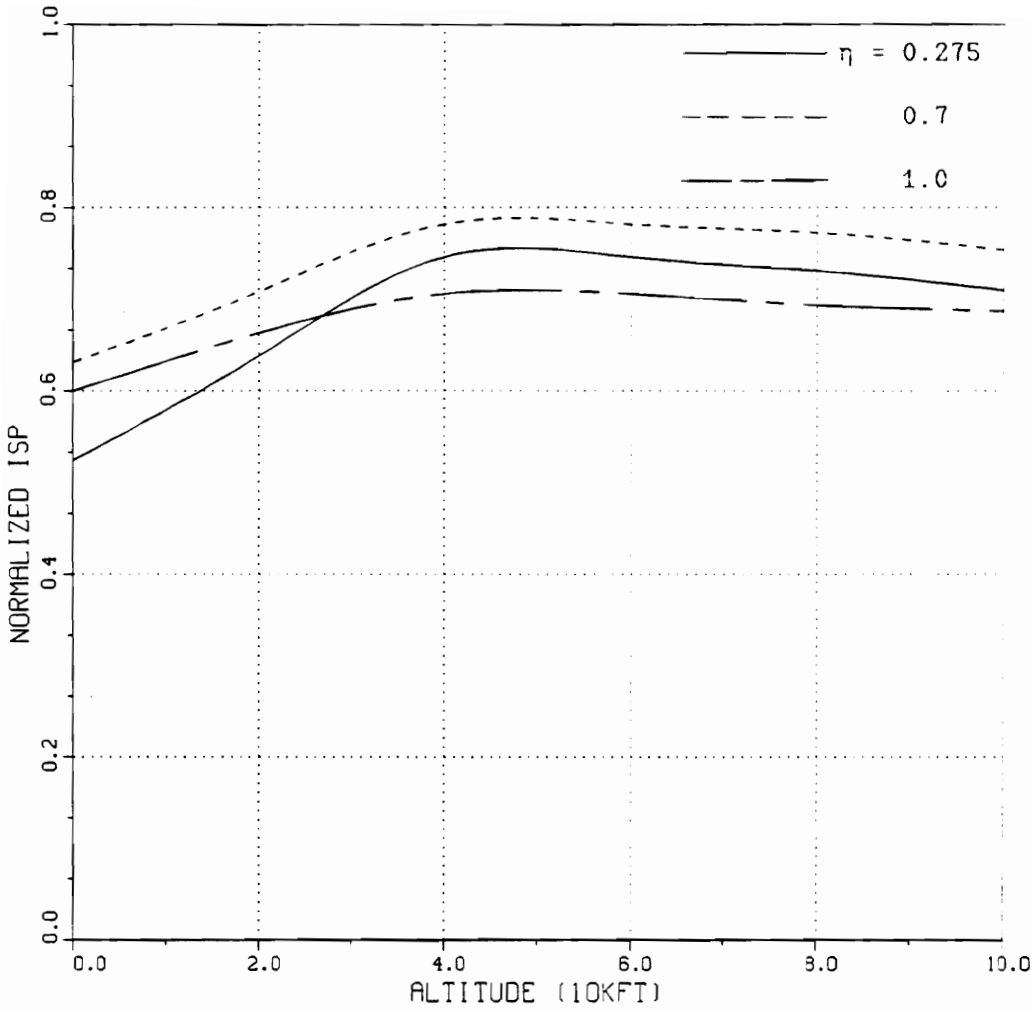

Figure A-10. Thrust Specific Impulse vs. Altitude:

M = 5, η varying

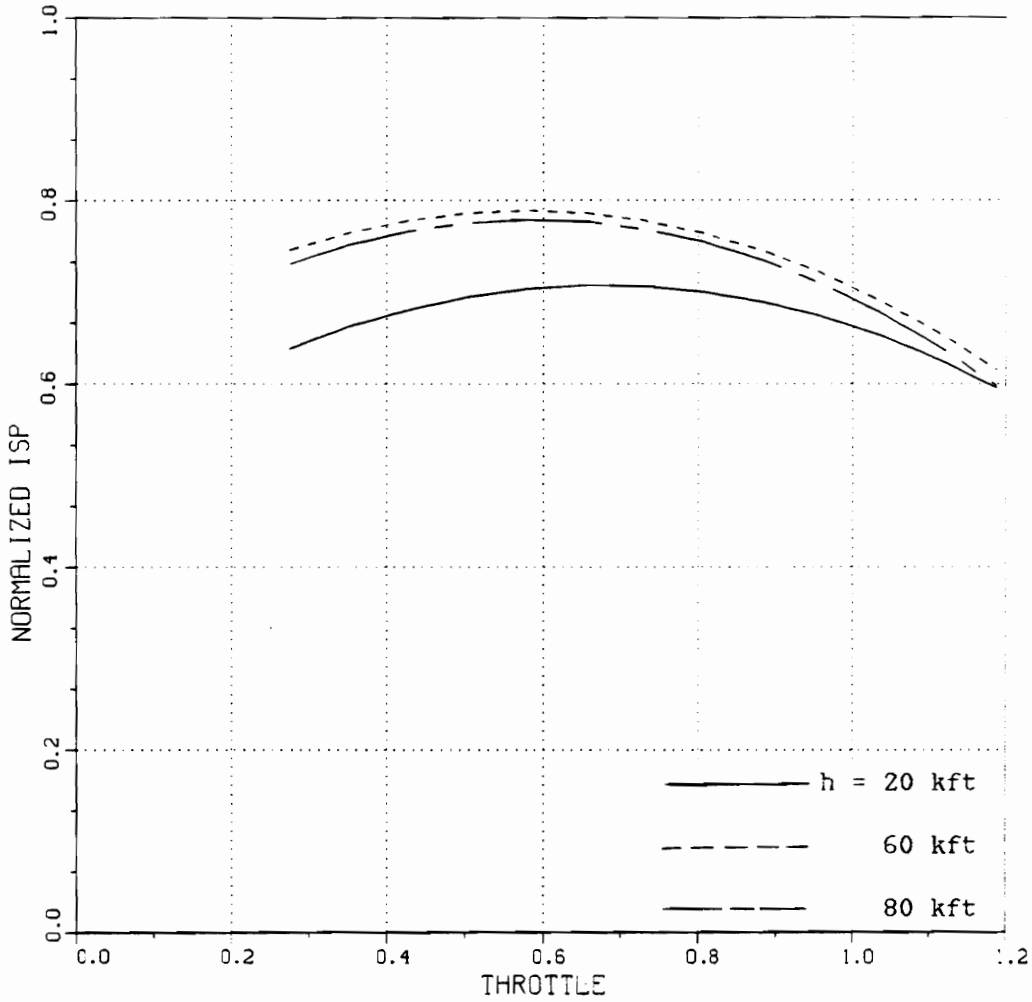

Figure A-11. Thrust Specific Impulse vs. Throttle:

M = 5, h varying

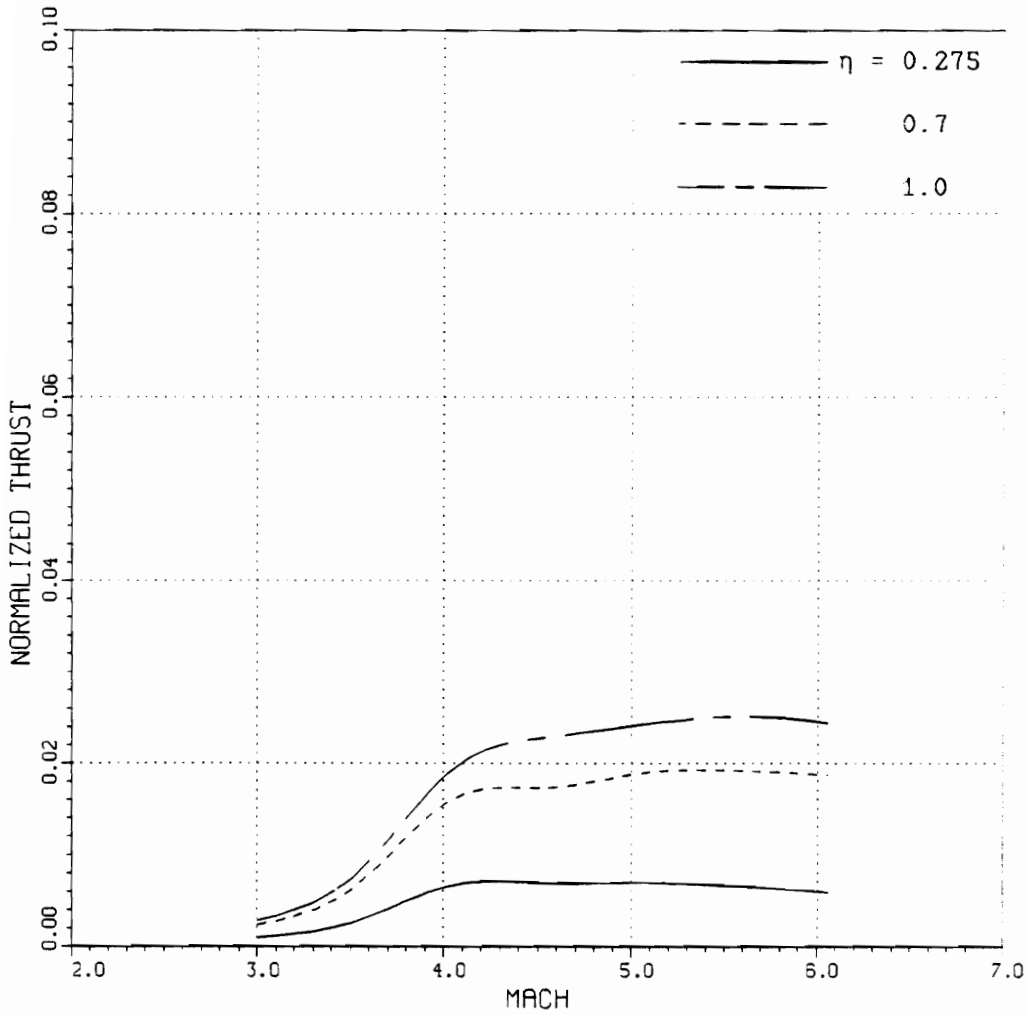

Figure A-12. Thrust vs. Mach: h = 80 kft, η varying

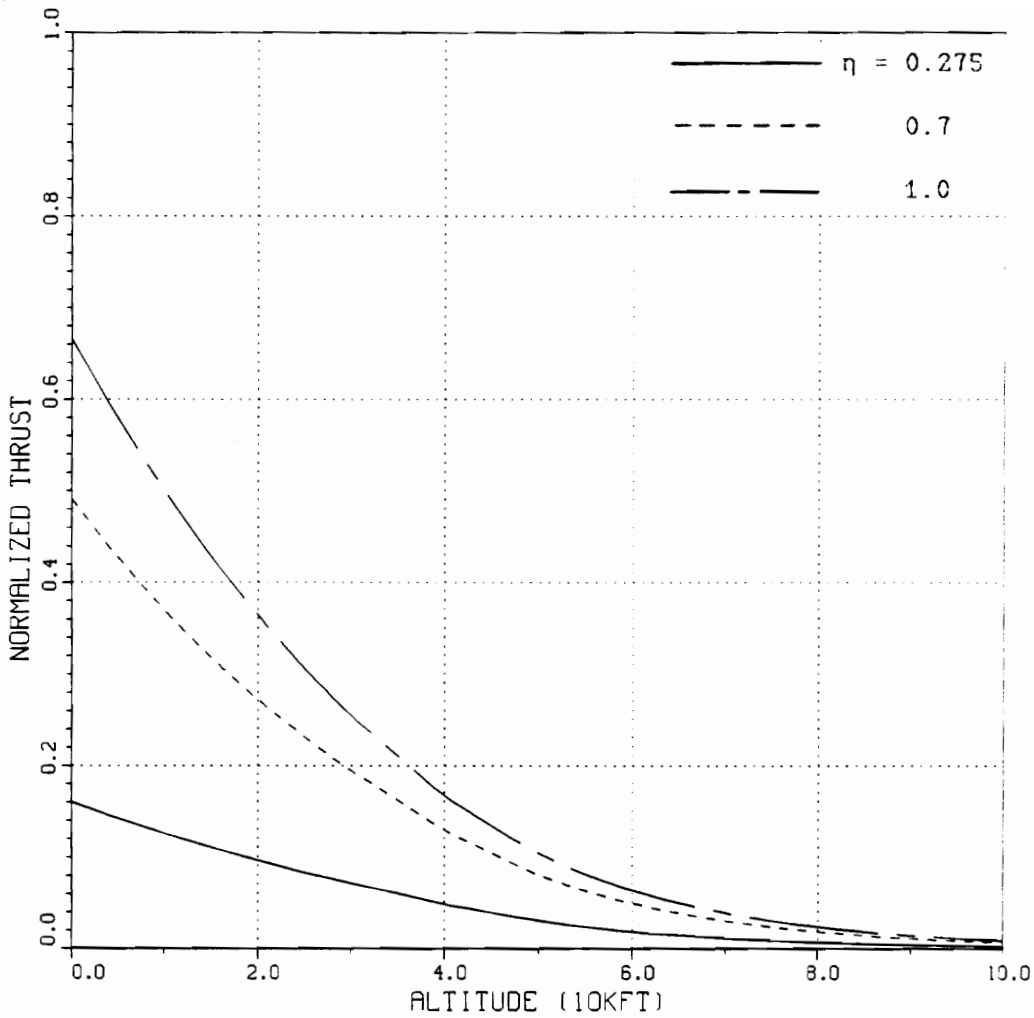

Figure A-13. Thrust vs. Altitude: M = 5, η varying

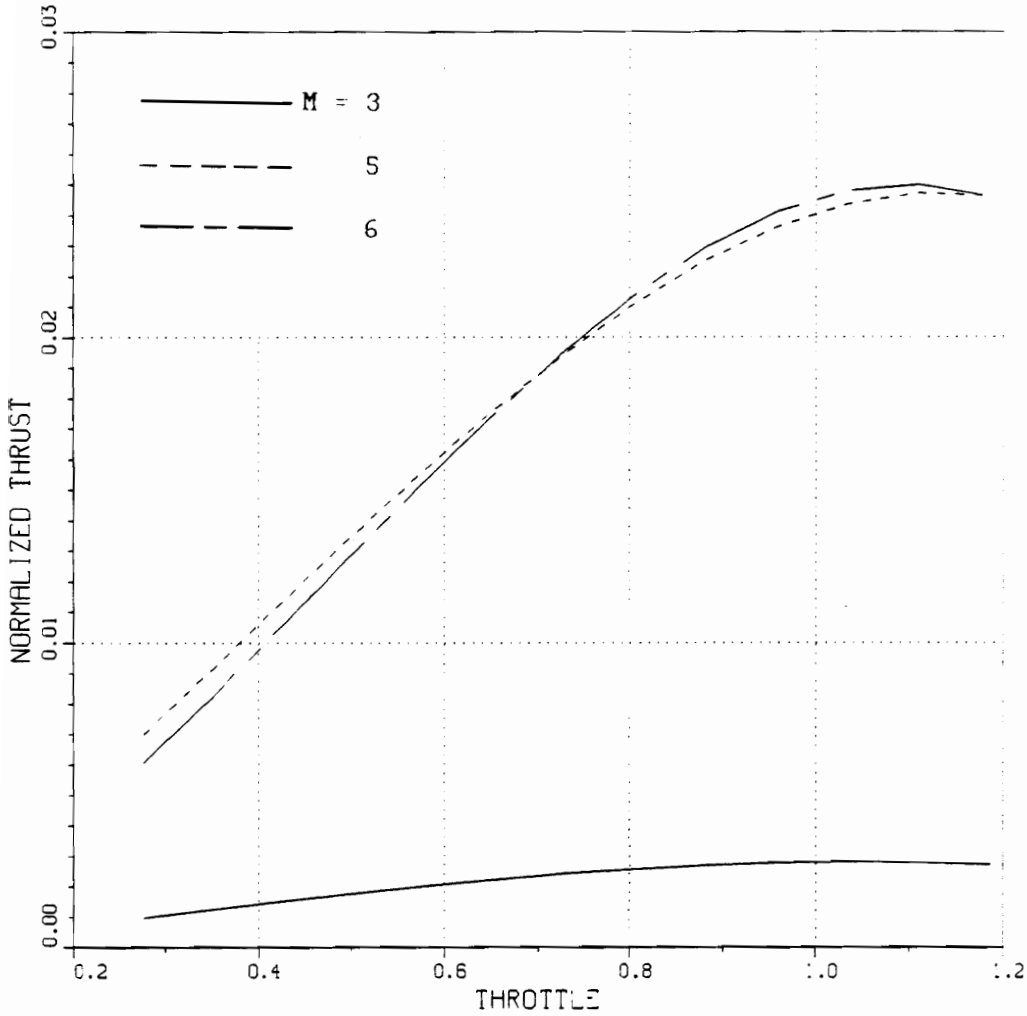

Figure A-14. Thrust vs. Throttle: h = 80 kft, M varying

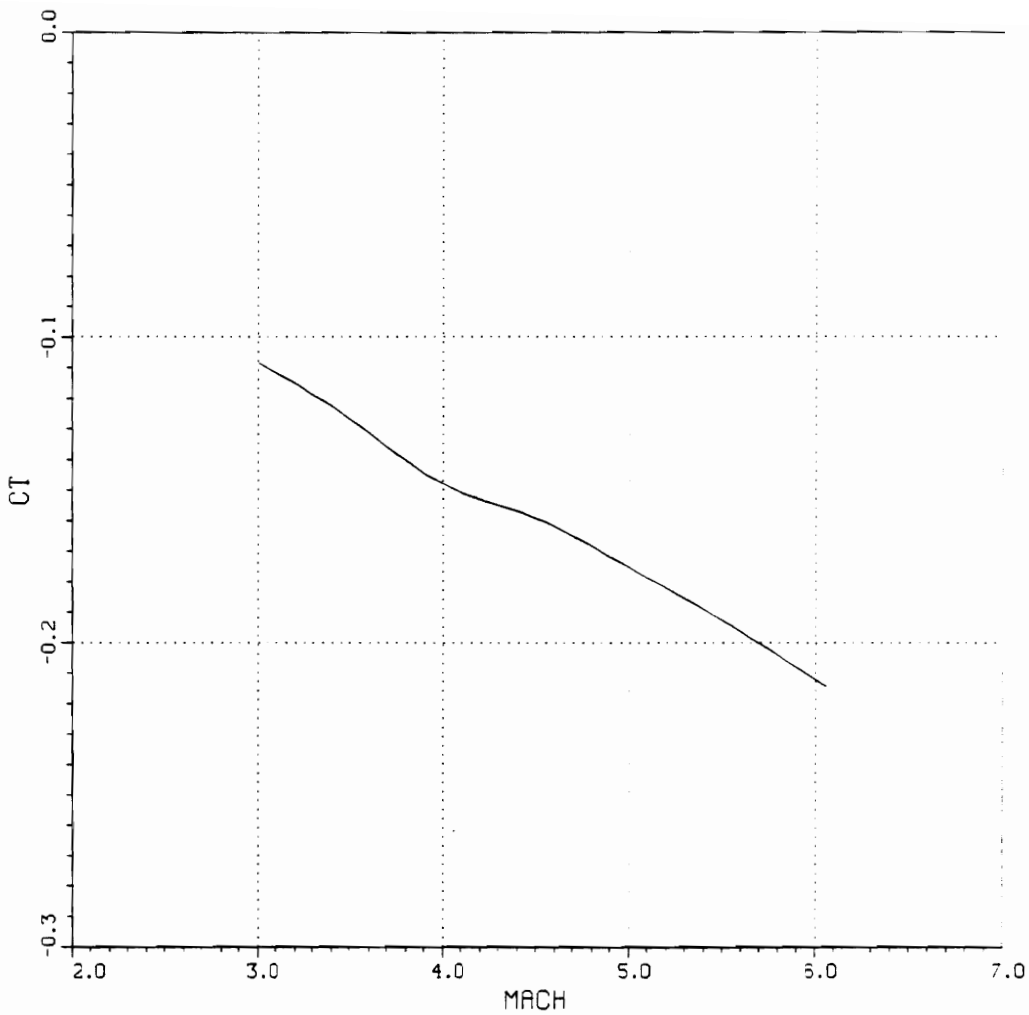

Figure A-15. Engine-Off Thrust Coefficient vs. Mach

VITA

The author was born in Seville, Spain in nineteen hundred and fifty-eight. She received a Bachelor of Science in Aerospace and Ocean Engineering in nineteen hundred and eighty-one from Virginia Polytechnic Institute and State University. During that time she also participated in the cooperative education program at the David Taylor Naval Ship Research and Development Center. She is currently an aerospace engineer with the Naval Surface Warfare Center.

This thesis has been written to meet the requirements of Master of Science in Aerospace Engineering at Virginia Polytechnic Institute and State University.